COMPUTATIONAL MODELLING OF FRACTURE AND DISLOCATIONS

Peter Szelestey

Dissertation for the degree of Doctor of Science in Technology to be presented with due to permission of the Department of Electrical and Communications Engineering, Helsinki University of Technology, for public examination and debate in Auditorium S4 at Helsinki University of Technology (Espoo, Finland) on the 4th of February, 2005, at 12 noon.

2

Abstract

Mechanical properties of solids bear great significance because of their importance in various fields of engineering and materials science. Fracture and plasticity are the two characteristic mechanisms by which materials permanently deform under external loading. Beside experiments and theoretical model calculation computational modelling greatly contributes to the understanding of these phenomena. This dissertation consists of various studies of topics related to these fields.

First, the branching instability of dynamic fracture is studied in a simple lattice model which describes a brittle material at mesoscopic length-scales. It is shown that the presence of anisotropy leads to a variation in the fracture pattern and crack tip velocity oscillations.

The second part of the thesis consists of atomic level computational modelling of dislocations using molecular dynamics method. Here, the interatomic potential plays a definite and relevant role. For that reason a semi-empirical, many-body embedded-atom potential is developed which turns out to be especially suitable for dislocation studies in fcc crystals, because of the realistic stacking-fault energies it predicts. Dislocation properties at the atomic level determine the micro-structure and in turn the plastic properties of materials. The static dislocation core structure is determined for dissociated dislocations in nickel and compared to analytical calculations. Furthermore, the effective Peierls stress, characterizing the dislocation mobility, and the variation in the dislocation structure through its motion is investigated for the screw orientation as a function of the separation distance of partials. Finally, the interaction of a dissociated screw dislocation and a vacancy type stacking-fault tetrahedron is studied. A wide variety of dislocation processes are found including bending and jog line formation, depending on the internal structure of the dislocation, the orientation and position of the defect.

i

ii

Preface

This thesis for the degree of Doctor of Technology has been prepared in the Laboratory of Computational Engineering (LCE), Department of Electrical and Communications Engineering of Helsinki University of Technology. The work has been funded by the Academy of Finland through the Center of Excellence programme.

I am foremost thankful to my supervisor Acad. Prof. Kimmo Kaski for continuing support and providing excellent conditions during the years of research at the LCE. Chronologically, the research work leading to this thesis has been started in cooperation with Dr. Pekka Heino and professor János Kertész, to whom I am especially grateful. As later the focus of research shifted toward atomistic simulations I was working with Dr. Leonel Perondi who helped me not only to get acquainted with the field of atomic level simulations but also giving useful ideas of further research directions. The most significant part of the research work was carried out in cooperation with Dr. Marco Patriarca, whose contributions and encouragement helped me through the more demanding part of the research leading to this thesis, and I am especially indebted to him. My colleagues at the LCE provided a very friendly environment and I would thank the valuable scientific and practical help from the senior researchers Dr. Michael Patra, Dr. Antti Kuronen and Dr. Mikko Kartunen, and my colleagues Anu Huttunen, Mirta Rodriguez, Maria Sammalkorpi, Fredrik Boxberg, Petri Nikunen, Markus Miettinen, Jukka-Pekka Onnela and Marko Sysi-Aho.

Finally I thank the support of my family and friends in Finland and abroad. Without their immense support this work would not have been possible.

Péter Szelestey

iv

List of Publications

This Doctoral Thesis reviews the author's research work on computational studies of mechanical properties of materials. It consists of an introductory overview, followed by the following scientific publications of the author.

I. P. Szelestey, P. Heino, J. Kertész and K. Kaski *Effect of anisotropy on the instability of crack propagation*, Phys. Rev. E **61** 3378 (2000)

II. L. Perondi, P. Szelestey *Structure of a dissociated edge dislocation in copper*, Mat. Res. Soc. Symp. Proc. **578** 223 (2000)

III. P. Szelestey, L. Perondi, M. Patriarca and K. Kaski *Modified EAM potentials for modeling stacking-fault behavior in Cu, Al, Au, and Ni*, International Journal of Modern Physics B **16** 2823 (2002)

IV. P. Szelestey, M. Patriarca and K. Kaski *Computational study of core structure and Peierls stress of dissociated dislocations in nickel*, Modelling and Simulation in Materials Science and Engineering **11** 883 (2003)

V. P. Szelestey, M. Patriarca and K. Kaski *Dissociated dislocations in Ni: a computational study*, Materials Science and Engineering A. **390** 393 (2005)

VI. P. Szelestey, M. Patriarca and K. Kaski *Computational study of a screw dislocation interacting with a stacking-fault tetrahedron*, Submitted to Modelling and Simulation in Materials Science and Engineering

Throughout the overview these publications are referred through the corresponding Roman numerals.

Authors contribution

The author has played a major role in all aspects of the research presented in the thesis. The author has developed all computations tools and carried out all numerical simulations except in Publication II where he contributed significantly to the numerical calculations. The author has prepared all manuscripts except Publication II, where, however, he actively took part in the preparation of the manuscript. The author has initiated the research lines leading to publications V and VI.

Contents

Chapter 1

Introduction

The mechanical properties of materials have always been under great interest since ancient times. Historically, in the Stone Age humans used bones, flints and other stone tools for practical purposes. Later on the processing of metals (melting, welding, casting, alloying) became a central technological factor of human advancement. Until modern times, progress has been based mainly on phenomenological and empirical study.

Materials Science [1] on the other hand aims to explain and determine the macroscopic properties (mechanical, thermal, optical, electrical and magnetic) of solids by studying their detailed micro-structure. It is a wide and essentially interdisciplinary subject including the fields of chemistry, physics, recently even biology and the more practically oriented metallurgy and mechanical engineering. The interdisciplinary character is partially due to the fact that the materials under study can be very different ranging from pure metals and their alloys, to fibers, ceramics, glasses, polymers and rocks. Furthermore, the subject is wide because of the several processes involved.

This thesis concerns the study of mechanical properties of materials. The most elementary mechanical property of solids is *elasticity*. A sufficiently small loading applied on a solid causes a reversible deformation. This deformation is generally described by the strain tensor ϵ_{ij} and the forces acting on the surface of a material by the stress tensor σ_{ij}. All solids are characterized by a regime in which the deformation is proportional to the applied stress, that is where linear elasticity is valid. In this regime $\sigma_{ij} = \sum_{k,l} C_{ijkl}\epsilon_{kl}$, where the elastic tensor C_{ijkl} characterizes the stiffness of the material in question, with some relations between its elements being determined by symmetry. It is well-known that the number of independent elastic constants is three in cubic materials and two in isotropic media, for which one can use e.g. the shear modulus, μ, and the Poisson ratio ν.

As one increases the stress of loading, materials can undergo *plastic*, that is permanent and irreversible, deformation, at the point signaled by the yield-stress. By applying further stress the material may suffer fracture, and ultimately break down. Materials characterized as being ductile undergo extensive plastic deformation before they break, whereas brittle materials have only limited plastic behaviour and break shortly after the elastic regime. Extreme examples for these types of behaviour would be silicon whisker as an ideal brittle material and pure gold as an example of ideally ductile material. This categorization is, however, somewhat vague because the same materials can also undergo brittle-ductile transition.

The material properties described above are characterized by various quantities: (i) the (yield)-strength describing how much stress the material can sustain until it deforms plasticly and (ii) the (fracture)-toughness, that is the resistance of the material against crack propagation, i.e. the ability to absorb plastic deformation. These characterizations can be illustrated by considering for example glasses and steel, both having high strength but steel having far superior toughness. Fracture and plastic deformation are only the basic behaviours to describe deformation. There are other more complex behaviours. For example, the time-dependent breakdown, a manifestation of progressive fracture due to cyclic loading, is generally referred to as fatigue and the slow, time-dependent plastic behaviour which takes place generally at high temperature is known as creep.

These macroscopic material properties ultimately depend on the atomistic and micro-scale structure. In crystalline materials, such as metals and alloys, plastic deformation is realized by the slip of crystallographic planes mediated by motion of dislocations or less significantly, by twinning of planes. In non-crystalline materials, such as glasses, the mechanism of plastic deformation takes place due to viscous behaviour, in which the stress is proportional not to strain but rather to strain rate $\dot{\epsilon} \sim \sigma$. This is characteristic of liquids, although the viscosity is several orders of magnitude larger. These materials are said to be visco-elastic, or visco-plastic to emphasize the occurrence of plastic deformation.

The present collection of research works concerns two (distinct) areas of mechanical and structural properties of materials: (i) brittleness and how it is revealed through instabilities in crack propagation, (ii) plasticity studied through both statics and dynamics of dissociated dislocations in metals, and a description of the corresponding atomistic properties. In addition, the thesis includes the work on the development of the semi-empirical interatomic potential used in atomistic simulations.

In this thesis we study structural properties of solids by using computer simulations, which can play an integral part in materials research beside the experimental and theoretical analytical approaches. Simulation can serve as a tool to understand phenomena unreachable for analytic calculation or experimental observation and

furthermore they can be used in computer-aided materials design in order to create new materials. The growing importance of computer simulation is based on the increasing demand of materials with exceptional mechanical properties, such as materials used in micro-electronics, aerospace industry or materials for nuclear applications. The rapid increase in computer power and the advance in simulation techniques have made the corresponding numerical computations more efficient and very large-scale simulations possible.

Chapter 2

Meso-scale fracture modelling

Fracture phenomena are one of the most studied branches of mechanical engineering because of their important technological aspects, with the general and main task in mind of preventing a material from breaking. One of the specific problems attracting special interest from the physics point of view is related to the dynamic instabilities observed in crack propagation of brittle materials.

2.1   Dynamical instability in brittle fracture

Continuum elasticity provides a general framework for fracture studies [2, 3]. In the fracture modelling of continuum elasticity the bulk material is adequately described as a continuum elastic medium. On the other hand, the vicinity of the crack tip is characterized by a diverging stress field, where the crack tip itself represents a singularity. In this region, the so-called *process zone*, continuum elastic description is no longer valid and thus the detailed atomic processes such as bonding between atoms become relevant. As the crack propagates a large amount of elastic energy, stored in the bulk material is dissipated. The key quantity in fracture mechanics is the phenomenological fracture energy Γ, defined as the energy required to create a unit area of fracture. In fracture engineering the main task is concentrated in determining the condition for cracks to propagate depending on the geometry of the system. According to the Griffith criterion, which is generally valid in the case of very sharp cracks, a crack starts to propagate, when the elastic energy in the bulk is sufficient for creating two surfaces at the tip. This means that Γ is at least equal to the energy of the two unit surfaces created in crack propagation.

From the linear elasticity theory point of view it is expected that the crack propagates in a straight line and its speed v reaches the limiting value of surface elastic waves c_R, also referred to as Rayleigh-velocity. In reality, however, crack motion

hardly reaches the theoretical Rayleigh-velocity and it shows several instabilities. This means that after the crack tip supersedes a critical velocity its propagation becomes increasingly complex, changing its direction forming rough surfaces and side cracks and producing radiating energy. In phenomenological terms, this can be explained as a dependence of the fracture energy Γ on the crack velocity v, and depending on that relation, the fracture process can be arbitrarily complex.

An example of dynamic instability was shown by Fineberg and co-workers, who have experimentally studied crack propagation in polymethylmethacrylate (PMMA), a glassy and brittle polymer. They found that above a certain critical threshold, at $v = 0.36c_R$, velocity oscillations appear with a dominant frequency [4, 5]. Additionally, above the critical velocity the crack surface structure changes, with a monotonic increase of the mean crack velocity. In their measurement, Sharon *et al* [6, 7] have identified micro-branching as the mechanism for the dynamic instability above the critical velocity. Near the crack tip side-branches, so-called daughter cracks are formed and propagate simultaneously with the main crack. These daughter cracks have a finite lifetime and beyond a certain length they stop propagating. As the crack velocity increases, the length and the density of daughter cracks increases accordingly. The typical size of these micro-branches was found to be in the 0.1-1 mm range with a log-normal distribution. The velocity of the crack tip shows oscillations correlated to the branching. An interested reader might find further information on the different instabilities in the review of Fineberg and Marder [8].

Computer simulations have been a useful tool for studying fracture. One way of modelling dynamic fracture is the large-scale atomistic simulations of the crack tip using Molecular Dynamics method. Abraham *et al* [9] have shown the existence of a dynamical instability at $v = 0.32c_R$ in a Lennard-Jones solid, where the instability produced was the change in the direction of the crack tip and oscillations in its velocity similarly to the experimental results [4]. Gumbsch *et al* [10] have studied crack propagation using different interatomic potentials. They found a terminal velocity well below the Rayleigh threshold, $v = 0.4c_R$ and branching instabilities at large loads whose details depend on crystal orientation and viscous damping. The brittle-ductile nature of fracture processes is also studied for example in Ref. [11].

While atomic simulations are limited in size, and especially in simulation time, mesoscopic simulation can be used as a tool to bridge the gap between the atomistic and macroscopic length-scales. In mesoscale simulations the essential physics is incorporated in a simple model that exhibits the main behaviour. An example of such simulations is the beam-lattice model used to determine the statistical properties of cracks in branching instability [12]. The Born-lattice model with Maxwell-type viscosity was used by Heino and Kaski [13] for modelling the crack branching
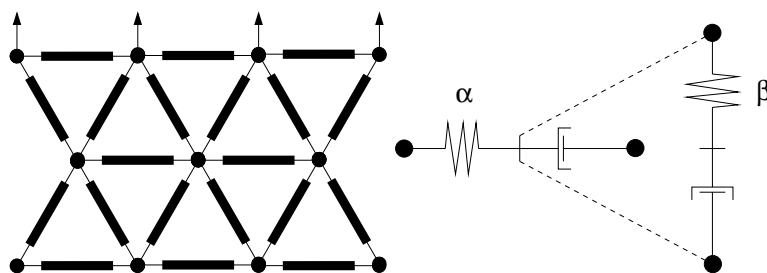
Figure 2.1: The triangular lattice model under mode I loading (left) and The Born-Maxwell type of force-field shown in a symbolic scheme (right).

phenomena and the effect of disorder characterized in the material parameters. The same model was used in this thesis and it is described in the following section.

2.2 Lattice model for crack branching

In order to simulate crack propagation and to observe the branching phenomena we have devised a 2D mesoscopic lattice model. In the lattice model the simulation describes the system at larger length-scale but at the cost of great simplification. Here the Born model [14, 15] is adopted as an appropriate lattice model for simulating an elastic medium. In the 2D case considered here mass points are located in a triangular lattice and a nearest neighbour interaction is defined by the following Hamiltonian,

$$H_{ij} = \frac{\alpha}{2}[(\mathbf{u}_i - \mathbf{u}_j) \cdot \mathbf{d}_{ij\parallel}]^2 + \frac{\beta}{2}[(\mathbf{u}_i - \mathbf{u}_j) \cdot \mathbf{d}_{ij\perp}]^2. \tag{2.1}$$

Here $\mathbf{d}_{ij\parallel}$ denotes the fixed unit vector connecting the sites i and j in the undisturbed lattice and similarly $\mathbf{d}_{ij\perp}$ is the unit vector perpendicular to it. The elastic interaction between neighbouring sites are described with spring constants α and β representing the longitudinal and angular stiffness. The lattice sites correspond to the center of a mesoscopic area with a size of about 10^{-6} m. The model satisfies the conditions of an elastic medium but without the rotational invariance [15]. This is however not very important in the case of the simulation set-up used in Publication I because of the lack of rotations.

The types of loading undergone by solid samples can be characterized in terms of different loading modes. For simplicity we use mode I loading, i.e. tearing, on the system, in which the crack faces are displaced in a direction normal to the
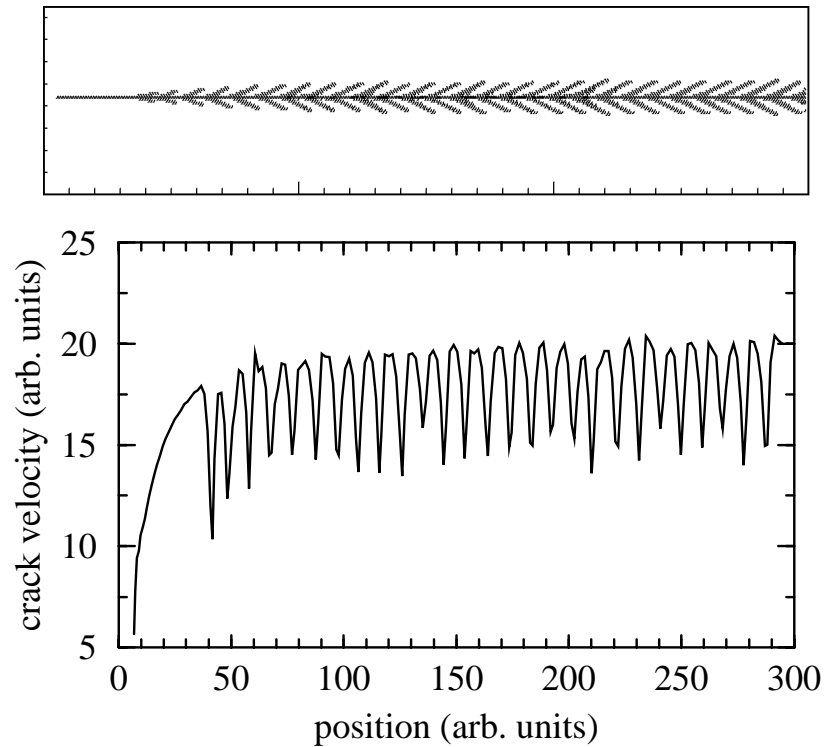
Figure 2.2: Fracture pattern in the isotropic Born-Maxwell lattice model (above) and the velocity oscillations of the crack tip (down). (Publication I.)

fracture line. Constant strain-rate is used in a way that the topmost layer is moved with constant velocity $\dot{\mathbf{u}} = const$ while the bottom layer is fixed, $\mathbf{u} = 0$, see Fig. (2.1). The bonds connecting the nearest neighbour sites break when the local strain exceeds a critical value set as a parameter in the model. The irreversible bond breaking brings non-linearity into the model. Because of the discreteness of the model the crack can only propagate perpendicular to the bonds. Modulation in the local material properties, such as disorder and anisotropy, are introduced in the model by variation of the elastic-spring constants. In the simulations there is an initial seed for crack introduced by breaking some bonds. The model also includes dissipative behaviour that is of time-dependent, viscous, Maxwell type. Thus the model is named as Born-Maxwell model. The implementation of the viscosity is carried out by distinguishing between displacements and elastic displacements,

connected by a phenomenological relation, of the following form,

$$\dot{\mathbf{u}}_{\mathrm{e},j} = \dot{\mathbf{u}}_j - \frac{1}{\tau}\mathbf{u}_{\mathrm{e},j} \; . \tag{2.2}$$

Correspondingly Eq. (2.1) is modified in a way that displacements $\mathbf{u}_i$ are replaced with elastic displacements $\mathbf{u}_{e,j}$. The role of dissipation has been previously studied in Ref. [16] on a square lattice and it was shown that the model can exhibit both brittle and ductile behaviour depending on the relation between the strain-rate and dissipation time. The Born-Maxwell model studied in Publication I is observed to represent the case of brittle fracture. The effect of increasing viscosity is a decrease of the intensity of branching and the length of daughter cracks.

The fracture pattern is shown in Fig. 2.2 to the isotropic case. Isotropy in this context means that material properties are equivalent along the three principal directions. Crack propagation in the isotropic model was studied in Ref. [13]. After the initial stage on both sides of the main crack so-called daughter cracks appear symmetrically with a regular period and the crack tip shows velocity oscillations. As new daughter cracks appear symmetrically at the crack tip, the velocity of the main crack drops significantly followed by the interval of acceleration and steady velocity until the next pair of side cracks are formed. The motivation of Publication I was to study the fracture process in the presence of anisotropy.

Chapter 3

Dislocations in metals

Dislocations are now known to play a fundamental role in materials science and to be essential for understanding the strength of crystalline materials. In the following, a general overview on dislocations, particularly in face-centered-cubic metals is presented.

3.1 Dislocations and plastic deformation

Already in the early 20th century, it was recognized that several properties of the crystalline materials cannot be explained simply from the perfect crystal picture, which was suggested by X-ray scattering experiments. The pivotal example is the strength of metals, for which the experimentally observed critical stress for plastic deformation is several orders of magnitude smaller, $\sigma \approx 10^{-3}\mu - 10^{-5}\mu$, than the estimated theoretical shear stress, as obtained e. g. by Frenkel's estimate $\sigma = \mu/2\pi$ [17]. Historically the discovery of the modern dislocation concept is associated to the independent works of Orowan, Polanyi and Taylor in 1934 [18]. It was then understood that a unit slip can be realized by dislocation motion along a crystallographic plane requiring little stress, in contrast to the slip of the whole plane, and that this would explain why metals deform easily. The name dislocation originates from the earlier work of Volterra about certain types of deformations of elastic continuum materials, some of which are actually dislocations whereas others are disclinations in the modern terminology. Later, dislocations have been experimentally observed and since then an immense research has concentrated on dislocations. For a detailed account of early development in dislocation theory see Chapter I in Ref. [19].

As referred to in the Introduction it is now widely established that plastic deformation in metals is mediated by the motion of dislocations. Perhaps the main
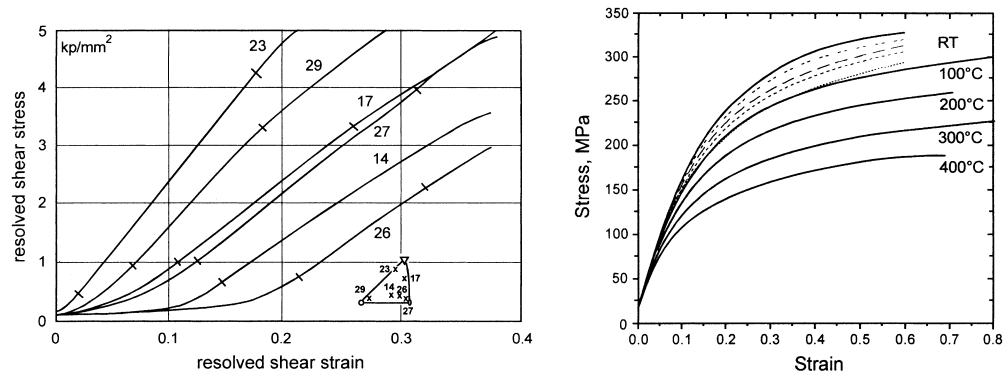
Figure 3.1: Left figure: Strain-hardening curves for a single Cu crystal divided into stages I, II and III. Each curve corresponds to a different orientation. Right figure: Compressive stress-strain relation for polycrystalline Cu and its temperature dependence. Figures are reproduced from Ref. [20]

motivation underlying dislocation theory has been the problem of work-hardening (strain-hardening) phenomena, the changes in the stress-strain relation measured when the material is put under external loading [20]. Throughout the deformation process several stages can be observed, each characterized by a distinct stress-strain relation. In single crystals, see Fig. 3.1, Stage I is characterized by a relatively flat stress-strain curve in which the material is deformed easily. Stage II is signaled by a sharp and generally universal hardening and in stage III a softening, i.e. dynamic recovery is observed with a parabolic stress-strain relation. In the theory of work-hardening [21] the different stages are explained in terms of dislocations. In the early region dislocations multiply rapidly and can move with easy-glide. Hardening results from dislocation accumulation and pile-ups that effectively block dislocation motion. These processes can depend on crystal orientation, material type, temperature, or, in polycrystalline material, on the grain size. Generally speaking most of the work done in plastic deformation is dissipated through dislocation motion and only a small amount is stored in the form of dislocation structure.

Dislocations also play a role in several related phenomena in materials science. Without giving a complete list, some examples are considered in the following. (*i*) The dislocation core represents a fast diffusion channel. (*ii*) Melting can be realized as a dislocation-mediated process [22]. (*iii*) The rate of crystal growth is significantly increased by the presence of screw dislocations ending at the surface, which serve as a seed for particle adsorption [23]. (*iv*) In hetero-structures it may
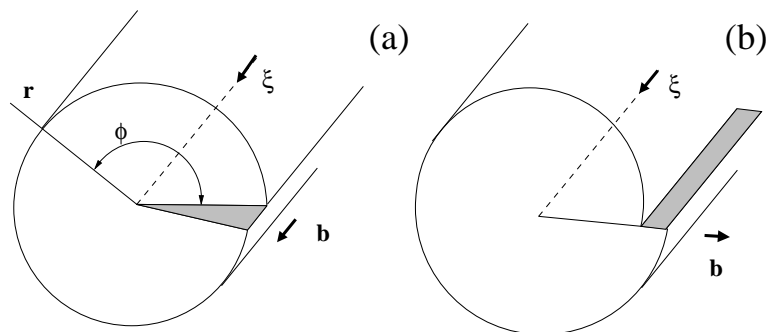
Figure 3.2: Illustration of a pure screw (left figure) and edge (right figure) dislocation in an ideal continuum elastic media. The dislocation line is denoted with dashed-line.

be energetically more favorable to form misfit dislocation rather than accommodate elastic strain. (v) In crack propagation dislocations are emitted from the crack tip [24].

3.2 Geometric and elastic properties

As Nabarro states in his book [17], the concept of dislocation is essentially a geometric one. Dislocations are line defects of an otherwise perfect crystal whose strength is characterized by the Burgers vector $\mathbf{b}$ [17, 19, 25]. The definition of a dislocation is either formulated in a continuum elastic medium or in discrete crystals. In the first case the Burgers vector is determined from a line-integral on a closed path taken on the local strain variation around the dislocation line,

$$\mathbf{b} = \oint \frac{\partial \mathbf{u}}{\partial l} dl \ . \tag{3.1}$$

Since in an elastic medium the displacement field is derivable from a potential field an arbitrary loop integral would give a value of zero, except if it encloses some singularity. Thus dislocations are topological defects similar to vortexes, and consequently a dislocation line is closed on itself or ends at a crystal boundary, free surface or grain boundary. When a dislocation with Burgers vector $\mathbf{b}$ dissociates into other dislocations, with Burgers vector $\mathbf{b}_1, \mathbf{b}_2, \ldots \mathbf{b}_N$, the total Burgers vector is conserved, $\mathbf{b} = \sum_i \mathbf{b}_i^N$.

In the case of a discrete lattice the Burgers vector is defined by taking a closed loop around the dislocation line, at far enough distance from the defect. Starting from the same point a similar loop is taken following the same local steps as
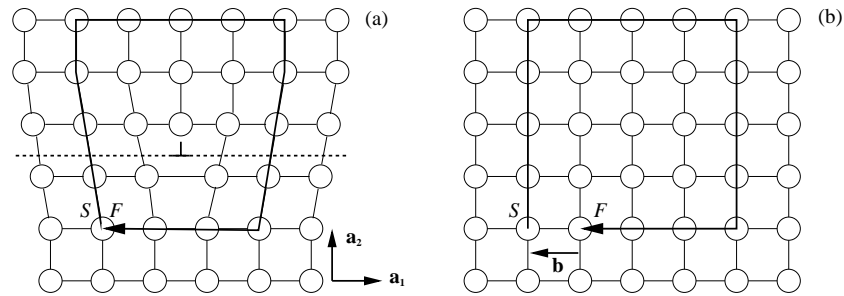
Figure 3.3: Atomic arrangements for (a) $b = [\bar{1}00]$ edge dislocation and (b) perfect crystal as seen by taking a 2D section of a simple cubic crystal. The circulation around the dislocation from S to F is marked with bold lines in both system and the difference defines the Burgers vector. The dislocation core is marked with symbol $\perp$ and the dashed line denotes the glide plane. The primitive unit lattice vectors are $\mathbf{a}_1$, $\mathbf{a}_2$ and $\mathbf{a}_3$, which goes out of the plane.

previously but assuming that the lattice is an undistorted perfect one. The difference between the two endpoints in the circulations defines the Burgers vector, see Fig. 3.3.

The direction for the dislocation line is denoted by $\boldsymbol{\xi}$, the sense vector, and the type of dislocation is determined by the relative orientation of $\mathbf{b}$ and $\boldsymbol{\xi}$. In the special cases when $\mathbf{b}$ is parallel to $\boldsymbol{\xi}$ the dislocation is a screw dislocation and when it is perpendicular it is an edge dislocation. The screw dislocation can have a right or left handed character when $\mathbf{b}$ and $\boldsymbol{\xi}$ point the same or opposite direction. These definitions can be given an intuitive meaning. For example an edge dislocation can be thought to be created by inserting or removing a half plane from a perfect crystal and relaxing the atoms around. Screw dislocation can be illustrated as the continuum medium is twisted along a fixed axis. In the general case, however, dislocations have a mixed character, that is they have a Burgers vector with both a screw and an edge component, and it is generally named as the acute angle enclosed by $\boldsymbol{\xi}$ and $\mathbf{b}$.

Any quantitative treatment of dislocations can be started by considering the mechanical response, that is the elastic stress and strain field around a dislocation. In the framework of continuum elasticity the stress and strain field around a perfect screw and edge dislocation can be analytically determined. The non-zero components of the stress and strain tensor around the dislocation decays as $\sigma \sim 1/r$ where r is the distance from the straight dislocation line, and the coefficient of proportionality depends on the geometry and the elastic constants. For example the

only non-zero component of the stress field around a perfect screw dislocation, as shown in Fig. 3.2, is simply

$$\sigma_{\theta z} = \frac{\mu b}{2\pi r} \, .$$

(3.2)

For a complicated curved dislocation the determination of the stress-field can be increasingly difficult but the general result is that dislocations produce a long-range stress field and have a long-ranged mutual interaction. When there are internal stress fields in the material, mobile dislocations rearrange themselves to effectively balance the stress field. Reasonably far from the dislocation line the distortion of the crystal is adequately described by elasticity theory, but when approaching the dislocation line the continuum elasticity description fails. The dislocation core is defined as the region of material where the crystal lattice has significant distortions and is practically of the order of a couple of lattice parameters.

The energy of a dislocation is proportional to the square of the Burgers vector. For this reason only dislocations with small lattice vectors are stable, as for a dislocation with larger $\mathbf{b}$ it is more favorable to dissociate into dislocations with smaller Burgers vector, with the full Burgers vector conserved, $\mathbf{b} = \sum_i \mathbf{b}_i$. This is formulated in the so-called Frank rule which states that the dissociation of a dislocation takes place if the condition $\mathbf{b}^2 > \sum_i \mathbf{b}_i^2$ is satisfied.

As mentioned above, plastic deformation happens primarily through the motion of dislocations. By applying an appropriate stress component on the plane, parallel to the glide plane, the dislocation can be moved. The force per unit length exerted by the stress is given by the Peach-Koehler formula [17],

$$\frac{\mathbf{F}}{L} = (\mathbf{b} \cdot \boldsymbol{\sigma}) \times \boldsymbol{\xi} \, ,$$

(3.3)

where $\mathbf{F}$, $\mathbf{b}$ and $\boldsymbol{\xi}$ are vectors and $\boldsymbol{\sigma}$ is the stress tensor. This means that the dislocation is moved by the external stress resolved on the glide plane and the direction of the stress is parallel to the Burgers vector.

There are two distinct types of dislocation motion. In glide motion dislocations move in the plane that contains both the dislocation line and the Burgers vector that is the glide-plane. Glide motion may require a critical stress, as the bonds in the core region must be broken and new bonds to be formed, but the motion is athermal and conservative with respect of the number of atoms and lattice sites. In Figure. 3.3 (a) the dislocation can glide horizontally in the $\mathbf{a_1}$ direction. Perfect screw dislocations have no definite glide plane and can exhibit cross-slip, that is the change of plane of motion. Climb motion is a mechanism in which the dislocation moves out of its glide plane. Basically it is a diffusion assisted process requiring the presence of impurities and thermal activation. In the example of the dislocation in Figure 3.3 (a) removal of the atom in the center of the dislocation core, or
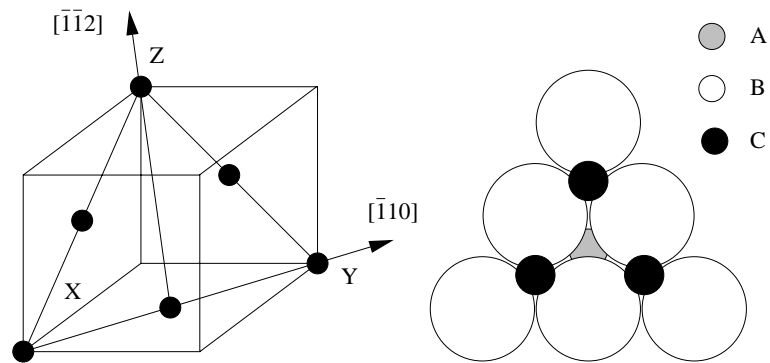
Figure 3.4: Left: conventional unit cell of the fcc lattice with some atoms forming a (111) plane. Right figure: the stacking sequence of close-packed (111) planes, in which atoms are imagined as hard balls.

equivalently the addition of a vacancy, represents a vertical motion with a lattice constant, i.e. a positive climb. Similarly an insertion of an interstitial in the core of the edge dislocation would move the dislocation in the negative $\mathbf{a_2}$ direction, thus producing a negative climb. It is noted that climb motion has relevance in creep phenomena. Defects capable of easy-glide motion are named glissile and those, which are not, sessile.

3.3   Dislocations in FCC crystals

Metals with face-centered cubic (fcc) structure include the technologically important Al and Ni and the precious metals Au, Ag and Cu. With the exception of Ir, fcc metals are ductile over a wide temperature range. Especially precious metals have excellent deformation properties and it is no surprise that they have been the first metals to be used since ancient times. Al and the precious metals are excellent conductors. These elements are technological important both in the pure and the alloyed forms composed with each other, such as CuAu and NiCu, or with other metals.

3.3.1   Dissociated dislocations

In the fcc lattice structure the conventional unit cell, with lattice parameter a, contains three extra atoms placed on the faces of the cell. Alternatively, the lattice can be built up by the stacking-sequence of close packed $\{111\}$ planes, as illustrated
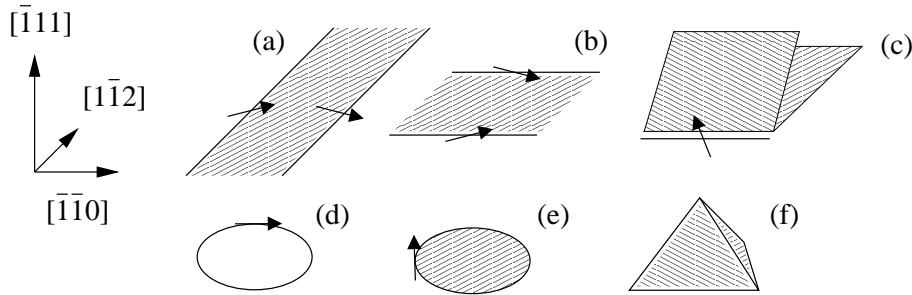
Figure 3.5: Different types of extended dislocations and defects in the fcc structure; $\mathbf{b} = \frac{1}{2}[\bar{1}\bar{1}0]$ dissociated screw (a) and edge (b) dislocation, (c) $\mathbf{b} = \frac{1}{6}[\bar{1}10]$ stair-rod dislocation (d) $\mathbf{b} = \frac{1}{2}[\bar{1}\bar{1}0]$ prismatic loop; (e) $\mathbf{b} = \frac{1}{2}[\bar{1}11]$ Frank loop; (f) stacking-fault tetrahedron (SFT). Bold lines note dislocations and shaded areas stacking-faults. The orientation of Burgers vectors are shown, with the exception of the SFT.

in Fig. 3.4. The standard notation for the Miller indices of planes and direction is followed in this thesis. The crystal structure, here particularly the fcc, determines the type of dislocations in the crystal. There are only a limited number of possibilities for the crystal slip direction. From minimum energy criteria the dominant slip system is the $\frac{1}{2}\langle 110 \rangle \{111\}$. This means that dislocations move on one of the four possible $\{111\}$ planes, following the general principle that the preferred slip planes are the most densely packed. The actual Burgers vector is one from the six possibilities of $\frac{1}{2}\langle 110 \rangle$ types. These four planes with the six edges build up the Thompson tetrahedron [17]. Correspondingly, there are four types of dislocation that is either edge or 30°, when the dislocation line is parallel to $\langle 112 \rangle$ and screw or 60° when the dislocation line is parallel to $\langle 110 \rangle$ direction.

One of the most characteristic aspects of dislocations in fcc crystals is generally that they dissociate into partials. The concept of partial dislocation was introduced by Shockley as a dislocation with Burgers vector that is not a lattice vector and thus not bounded by a perfect crystal but rather a plane defect such as stacking-fault. An intrinsic stacking-fault is created from a perfect crystal by removing a close packed plane. For example removing an A plane from the $ABCABC$ sequence in Fig. 3.4 and then relaxing the system results in the stacking-sequence $ABCBC$. There are other plane defects such as twinning and extrinsic stacking-faults which are not studied in this thesis. A typical dislocation dissociation reaction for a perfect

dislocation, $\mathbf{b}_1$, into Shockley partials, $\mathbf{b}_2$ and $\mathbf{b}_3$, of type $\frac{1}{6}\langle 112 \rangle$ is

$$\frac{1}{2}[\bar{1}\bar{1}0] \rightarrow \frac{1}{6}[\bar{1}\bar{2}1] + \frac{1}{6}[\bar{2}\bar{1}\bar{1}] + \text{SF}\,, \tag{3.4}$$

where SF denotes the intrinsic stacking-fault region connecting the two partials. The Burgers vectors of partials have magnitude $b_{2,3} = a\sqrt{6}/6$ and usually have mixed character. For example a perfect edge dislocation dissociates into two $60°$ partials, and a screw dislocation into two $30°$ partials.

In the simplest description of the dissociated dislocation the partials are assumed to be infinite straight dislocations in an isotropic elastic medium. The equilibrium distance is computed as the balance between the repulsive elastic forces and the attraction caused by the positive stacking-fault energy. For a general dislocation of angle ϕ, the separation distance is

$$d_0 = \frac{\mu b_{2,3}^2}{8\pi\gamma_{\text{I}}} \left(\frac{2-\nu}{1-\nu}\right) \left(1 - \frac{2\nu \cos 2\phi}{2-\nu}\right)\,, \tag{3.5}$$

where μ is the shear modulus, ν is the Poisson ratio and γ_{I} is the intrinsic stacking-fault energy, see Eq. (10.15.) in Ref. [17]. It follows that d is inversely proportional to γ_{I}, so that materials with high γ_{I} such as Al and Ni have a small separation distance. Depending on the orientation, d increases monotonically from the screw case $\phi = 0$ to the edge case $\phi = \pi/2$. In reality, with the exception of tungsten, metals are generally anisotropic. Anisotropy can be characterized in terms of the anisotropy factor $A = 2C_{44}/(C_{11} - C_{12})$ and it can vary depending on the material. For Al it is close to one, indicating a moderate anisotropy but for other fcc metals the anisotropy can be significant, i.e. $A \approx 2 - 3$. For a proper description of dislocations, anisotropic effects need to be taken into account. The case of a straight dislocation in an anisotropic medium represents a difficult mathematical problem (see Chapter 13. in Ref. [17]). The calculation of the splitting distance was carried out by Teutonico [26, 27]. In the anisotropic case, a closed form of the analytical solution for the separation distance is possible only for special directions. When the separation distance is large, $d \gg b$, i.e. several times the value of Burgers vector, the description based on linear elasticity, the Volterra dislocation picture, is adequate. However, as separation distance becomes small, the finite width of the dislocation core needs to be taken into account.

3.3.2   Defect clusters

So far we have considered straight dislocations. There exist defect dislocations formed by vacancies or self-interstitials. Vacancies and self-interstitials are the

simplest (point) defects, vacancies being created by removing an atom and self-interstitials by adding an extra atom in the crystal. At finite temperature a material necessarily contains impurities as for example the number of thermally activated vacancies at equilibrium is

$$N = N_{tot} \exp(-E_v/k_bT) \exp(S_v/k_b), \qquad (3.6)$$

where N_{tot} is the total number of atoms, E_v is the vacancy formation energy and S_v is the thermal (vibrational) entropy term, see Ref. [28]. Dislocation loops can be constructed by removing a circular area of a {111} plane and relaxing the atoms from the crystal. This corresponds to the process of accumulation and coalescence of vacancies. In this way a vacancy dislocation loop is obtained that bounds a stacking-fault region inside, because of the missing plane inside the loop. This type of dislocation loop has a Burgers vector $\mathbf{b} = \frac{1}{3}\langle 111 \rangle$. In contrast to the Shockley partials these are Frank partials that are perpendicular to the plane of the dislocation loop. Similarly Frank loops can be constructed from interstitials. A prismatic loop is a dislocation loop that is bounded by an otherwise perfect crystal in contrast to a Frank loop, and the Burgers vector is in the plane $\mathbf{b} = \frac{1}{2}\langle 110 \rangle$. On the other hand, prismatic loops can be created by Frank loops by some un-faulting mechanism, for example as a result of a moving dislocation. They can be imagined as straight dislocations bent and reconnected with themselves, see Fig. 3.5.

Stair-rod dislocations are bounded by two stacking-faults on different {111} planes. The configuration can be acute, as shown in Fig. 3.5 or obtuse depending on the angle between the corresponding planes. A stair-rod dislocation can be a result of the dislocation reaction of partials on two dissociated dislocations on different planes. For example in Fig. 3.5 (c) a dissociated screw dislocation on the $(1\bar{1}\bar{1})$ and $(\bar{1}1\bar{1})$ plane can form a stair-rod dislocation. Stair-rod dislocations are sessile and represent a hard-object, so called Lomer-Cottrell lock, on dislocations moving on both planes it extends.

Stacking-fault tetrahedron (SFT) defects are bounded by four stacking-fault plane on all {111} planes. These defects can be explained as the six stair-rod dislocation forming the edges of a perfect tetrahedron. SFT can develop from a triangular Frank loop.

All of the above is only a short account on the type of several extended dislocations present in fcc crystals. An extensive list of these dislocation defect configurations can be found e.g. in Ref. [29] and a more detailed account of their description in Ref. [17], Chapter 10.

Experimental evidences show that in different materials different types of defects are dominant. In fcc materials the most common defects are stacking-fault tetrahedra and in bcc metals they are interstitial loops, depending on the defect

inducing processes [30]. The typical source of defect formation is either heavy plastic deformation [31] or irradiation [32]. This gives a strong motivation for studying defects in nuclear materials, in which a large number of defects formed through irradiation change the material properties, which on the other hand should sustain extreme mechanical conditions, such as e.g. high pressure and temperature.

The stability and the destruction processes of the defects described above have attracted much interest, especially in the context of the experimentally observed clear bands in deformed materials [33]. Analytic model calculations based on linear elasticity have been used to study destruction or transformation into different types of defects. In these processes the stress field or the direct interaction of a moving dislocation can be an important factor. The interaction process of a glissile dislocation with a perfect or truncated SFT, by using linear elasticity, has been studied in Ref. [34, 35]. It was shown that the elastic field of the moving dislocation by itself is not enough to transform the defect suggesting that dislocation reactions might play an important role in SFT destruction.

3.3.3   Stacking-fault energies

Because of the abundance of extended dislocations bounded by stacking-fault regions in FCC metals, stacking-fault energies have an enormous importance. Stacking-fault energies are very sensitive quantities. For comparison, typical metal surface energies are of the order of J/m^2, depending on the orientation, while stacking-fault energies are in the range of $\gamma_I = 10 - 200 mJ/m^2$, where for example gold and copper have low SFE, about $\gamma_I = 30 - 40 mJ/m^2$ and aluminum and nickel high ones $\gamma_I = 100 - 150 mJ/m^2$.

The easiest way to understand stacking-fault energies in closed-packed crystals is to consider a central-force, hard-sphere model, where atoms are imagined as hard balls with attractive force between them. Taking into account first and second nearest neighbour shells, there is no difference between fcc and hcp structures, since both have 12 and 6 atoms in the corresponding shells. Beyond, the number of atoms included in the shells depends whether it is an fcc or hcp structure and thus one of them is favored energetically. In Publication III we use a cut-off range, to ensure the hcp-fcc stability and to obtain physically reasonable stacking-fault energies. A more systematic way of incorporating the stacking-fault energy is within the tight-binding picture. In this case the higher-order momenta determine the value of the stacking-fault energy [70, 82].

The concept of generalized stacking-fault energy (GSF) – or gamma surface – has been introduced by Vitek [83]. The GSF-surface is the energy surface obtained by cutting a perfect crystal into half and displacing two half-bodies along the cut. When the displacement is $a(\sqrt{2}/4; \sqrt{6}/12)$, which corresponds to a Shockley
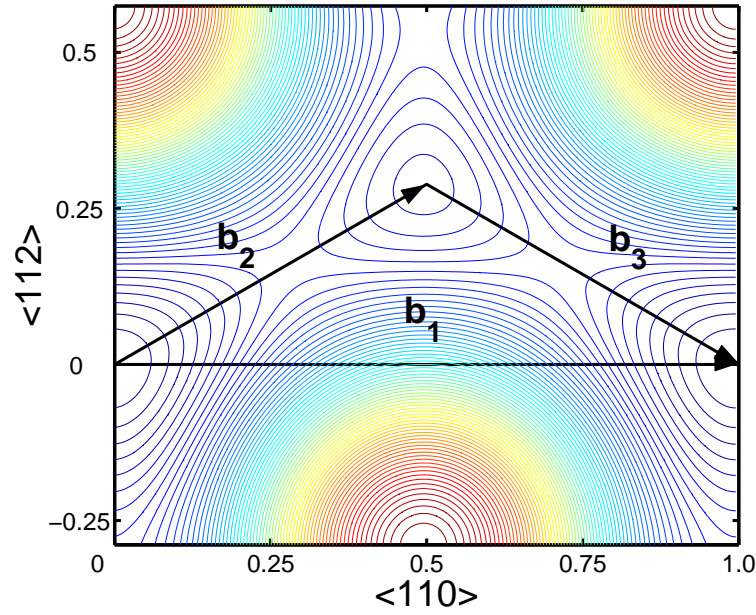
Figure 3.6: The generalized stacking-fault energy surface for Ni from the model potential of Publication III. The coordinated axes are normalized with the factor $a\sqrt{2}/2$. The Burgers vectors corresponding the dissociation process of a perfect dislocation b_1 into partials b_2 and b_3 according to Eq. (3.4) are shown.
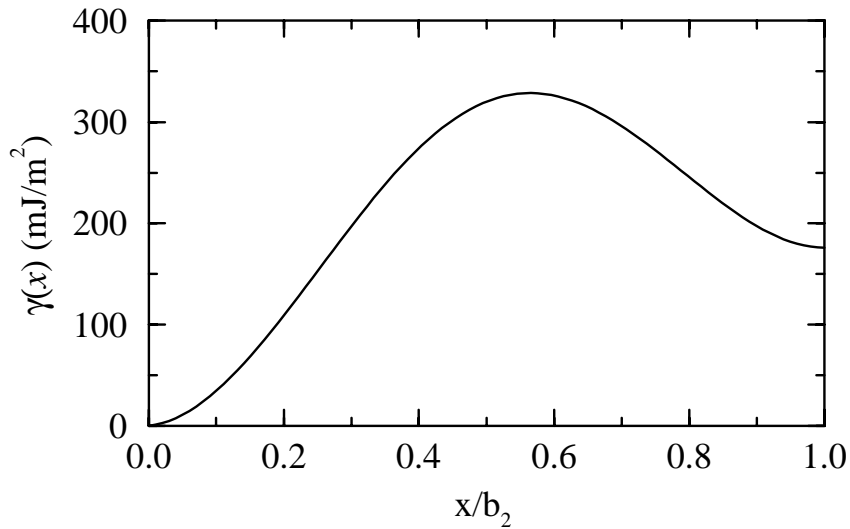
Figure 3.7: The GSF energy for Ni from the model potential of Publication III measured along the b_2 direction.

partial $\frac{1}{6}\langle 112 \rangle$, one obtains the value of intrinsic stacking-fault energy γ_I. The importance of the GSF is based on the fact that the atomic restoring force $F(x)$, as will be mentioned in the context of Peierls-Nabarro model, can be computed from the gradient of the GSF as

$$\mathbf{F}(x) = -\nabla\gamma(\mathbf{r}) . \tag{3.7}$$

The GSF-surface reflects the symmetry of the lattice. There are special points, such as the maximum and the saddle point, that are important for the parametrization and characterization of the GSF. In particular, the local environment near the origin of the GSF-surface represents the small shear strain and corresponds to the elastic limit.

The calculation of generalized stacking-fault energies from the first principles density functional theory are now available, see e.g. Ref [84]. Lu and Kaxiras [49] have compared certain paths on the GSF-surfaces calculated from density functional method and EAM, with the general conclusion that EAM-type potentials are capable of describing both the elastic limit and the intrinsic stacking-fault energy, even though they can overestimate it in intermediate points.

3.4   Effect of crystal structure

In the previous section we dealt with dislocations in an ideal continuum elastic medium. This approach has its main limitation in the fact that the dislocation core cannot be described through elasticity theory. In reality the dislocation exists in a crystal structure and the effect of the lattice periodicity needs to be taken into account. The simplest model is the Frenkel-Kontorova model [36] in which the dislocation is modeled as a set of particles coupled by nearest-neighbour elastic interaction and moving in a periodic potential. However, probably the most successful model which takes into account the discreteness of the crystal structure and describes the core structure and mobility of dislocation, is the so-called Peierls-Nabarro model.

3.4.1   Core structure

In the Peierls-Nabarro model the dislocation structure is described by a continuous disregistry function $f(x)$ – or its derivative, i.e. the misfit function $\rho(x)$ – rather than by a localized dislocation $\rho(x) = \delta(u - x)b$ as used in a continuum elasticity description. The main assumption of the model is that the dislocation is characterized by two relevant energy terms. The first one is the elastic energy due to a finite density of dislocations and is essentially a volume energy term. The second

energy term is the so-called misfit energy which results from the generally non-linear atomic interactions in the glide plane where the dislocation extends. This is characterized by the the nonlinear restoring force $F_b(x)$, which in the simplest form can be approximated as a sinusoidal function. Assuming that at equilibrium the stresses arising from the two terms are equal one obtains the Peierls-Nabarro integro-differential equation, which for a single dislocation reads as follows

$$\frac{K}{2\pi} \int_{-\infty}^{+\infty} \frac{1}{x-x'} \frac{df(x')}{dx'} dx' = F_b(f(x)) \,. \tag{3.8}$$

Here K is an appropriate elastic constant, the pre-logarithmic energy factor and the boundary conditions are $f(-\infty) = 0$ and $f(-\infty) = b$. In the general case $\mathbf{F}_b(\mathbf{f}(x))$ and $\mathbf{f}(x)$ are vectors with two components and $\mathbf{K}$ a tensor quantity. On the other hand in the 1D case with a sinusoidal restoring force, with amplitude $\tau_{\max}$ and $F(x) = \tau_{\max} \sin(2\pi x/a')$, Eq. (3.8) can be solved analytically with a remarkably simple solution,

$$f(x) = \frac{b}{\pi} \tan^{-1}\left(\frac{x}{\zeta}\right) + \frac{b}{2}, \tag{3.9}$$

where $\zeta = Kb/4\pi\tau_{\max}$. This well-known formula, first formulated by Peierls, is not only used in the context of the Peierls-Nabarro model but is also applied in interpreting simulation and experimental results. It shows that the singularity, present in the continuum elastic description, is eliminated from the dislocation core and at large distances the elastic field agrees with the result of elasticity theory.

3.4.2 Peierls stress

The Peierls-Nabarro model can be used for calculating the mobility of a dislocation, due to the lattice resistance acting through the Peierls stress. The Peierls stress is defined as the minimum stress required to move athermally a straight dislocation in an otherwise perfect crystal. It is derived by assuming that a dislocation, characterized by the disregistry function calculated from Eq. (3.8), experiences a variation in the misfit energy $W(x)$ through its motion in x direction. In this case the misfit energy is calculated at discrete lattice points on the glide plane. The Peierls stress is then obtained from the maximum force per unit length as

$$\sigma_{\mathrm{PN}} = \frac{1}{b} \left| \frac{d}{dx} W(x) \right|_{\max} \,. \tag{3.10}$$

In the case of fcc metals this definition is satisfactory but there are more complicated Peierls potentials, for example in the case of $\frac{1}{2}[111]$ screw dislocations in bcc
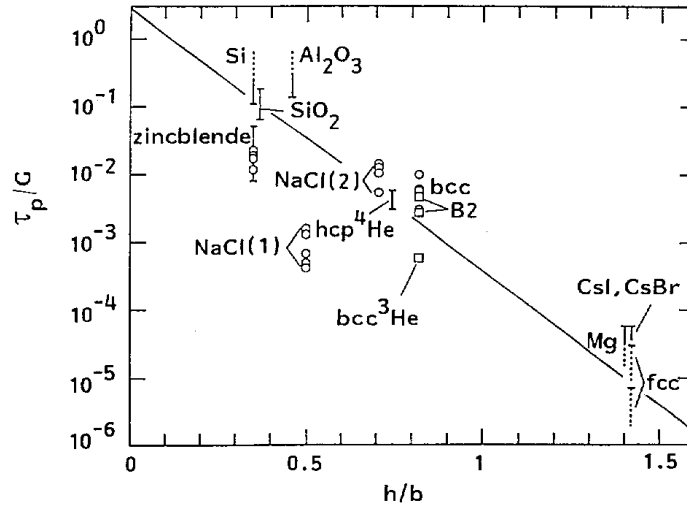
Figure 3.8: Experimental values for Peierls-Nabarro stress, σ_{PN} from Ref. [37] measured in units of shear modulus, τ_p/G, as a function of distance between glide planes relative to the Burgers vector h/b for several materials.

crystals which show a definite asymmetry and consequently two different Peierls stresses depending on the glide direction. The calculation of Peierls, corrected by Nabarro, leads to the value of the Peierls-Nabarro stress as follows

$$\sigma_{PN} = \frac{2\nu}{1-\nu} \exp(-4\pi\zeta/b) \,. \tag{3.11}$$

Qualitatively Eq. (3.11) shows that the barrier for dislocation motion is exponentially decaying on the core width and can be very small compared to the stress required for a crystal slip in a perfect crystal.

It should be noted that the Peierls-Nabarro-model is ambiguous in the sense that it uses both a continuous and discrete description. While the dislocation structure is determined for a continuous function, for the calculation of Peierls stress a discrete summation is used. Furthermore in the original calculation the dislocation structure is assumed to be fixed and internal relaxation is not taken into account. The critical stress has been a research subject over several decades and different estimates have been obtained starting from different assumptions which lead to a dominant term in the critical stress $\sigma_{PN} \sim \exp(-2\pi\zeta/b)$ as in Huntington [38] or

$\sigma_{\mathrm{PN}} \sim \exp(-4\pi\zeta/b)$ as in the original treatment. A comparison of these estimates with experimental data is in the review paper by Nabarro [39].

There is extensive literature concerning the Peierls-Nabarro model. Without trying to be complete, here we give some recent developments. Recently, Joós and Duesbery [40] have re-examined the classical Peierls-Nabarro equation and have shown that its validity can be extended to the case of narrow dislocation cores. Schoeck has used a variational principle [41, 42, 43, 44, 45], with parametrized functions for both the disregistry function, the Peierls-Nabarro solution ansatz and the generalized stacking-fault energy, to carry out a 2-dimensional study which takes into account anisotropic effects and the relaxation of the dislocation structure. This approach has been applied to both perfect and dissociated dislocations. It was shown that by taking into account the core effects the separation distance in dissociated dislocation leads to a correction compared to the elastic theory [42]. Some of the effects studied in the analytic calculations are re-examined in Publication V. Mryasov *et al* [46, 47] have also been using a similar variational method, with generalized stacking-fault energies, but with a different parametrization of the disregistry function. Bulatov and Kaxiras proposed a semi-discretized version of the model [48] in which the disregistry function is approximated by step-functions positioned around atoms. This model has been applied to both dislocation structures [49] and to study the effect of vacancies on dislocation mobility [50]. A fully discretized version of the model was developed by Ohsawa *et al* [37], in which the elastic interaction is logarithmic instead of the inverse function of the classical Peierls-Nabarro model in Eq.(3.9). Finally, the Peierls-Nabarro concept has been extended to non-planar dislocations [51].

The Peierls stress depends strongly on the crystal structure. For fcc crystals it is very small, whereas its value increases when moving to bcc metals and covalent crystals, see Fig. 3.8. The experimental determination of the Peierls stress can be made either from flow stress measurements which signals the onset of plastic deformation and thus the point at which dislocations start being mobile. Alternatively, σ_{P} is determined via the kink-pair formation energy, from the Bordoni-peak in internal friction measurements [52].

These arguments concern the zero temperature case for straight dislocations. At finite temperature dislocation motion is easier due to the motion of thermally activated kink-pair formation. Kinks are short dislocation segments that connect other dislocation segments lying in a different Peierls potential. The mechanism of dislocation motion by kink-pair formation is summarized in the following, see Fig. 3.9. At the beginning the originally straight dislocation is under the action of external stress which is not large enough to move the dislocation out of the Peierls valley. Because of thermal activation, it is possible for a kink-pair to develop, and move to the neighbouring Peierls valley. When the kink-pair is fully developed
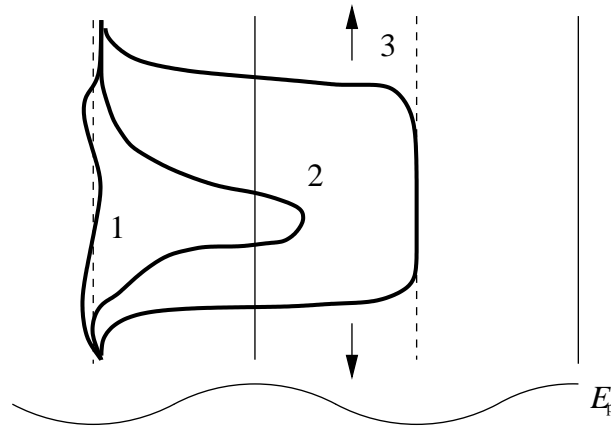
Figure 3.9: Motion by kink-pair formation, according to the following stages: (1) the dislocation is initially confined in a local Peierls valley (dashed line), (2) due to thermal activation a kink-pair gets through the energy barrier (continuous line), (3) the developed double-kink can now move in the directions of the arrows.

it can move along the valley with very little lattice resistance, characterized by the second-order Peierls stress which is much smaller than the first-order Peierls stress. When the kinks run along the whole dislocation, it means that a dislocation has moved a distance a'.

In fcc materials there is a contradiction between the Peierls stress values obtained from the onset of plastic deformation and internal friction measurements. For example, Benoit *et al.* [53] have found that in fcc Al and Cu the mobility of dislocations remains high at low temperature as compared to the estimates based on the Peierls stress from the kink-pair formation energy in the Bordoni peak of internal-friction measurement. A mechanism based on the internal structure was proposed to resolve the paradox. When the separation distance d is an integer multiple of the periodicity of the Peierls potential a', the dislocation needs to surmount the Peierls stress for a partial but on the other hand when d is a half-integer multiple of the period a' the required stress can be close to zero, as one partial can aid the motion of the other one. For a special half-integer case $d = 1.5a'$ Schoeck [54] has shown that the effective stress can be significantly smaller, though not zero. In the Volterra dislocation picture, when the dislocation is modeled as the coupled motion of two partials, this effect has been validated by Schoeck and Püschl [55]. In Publication V the question of the effective stress of a dissociated dislocation is addressed and studied with atomistic simulation.

Chapter 4

Atomistic level materials simulation

Traditionally, Materials Science research relies primarily on experiments and theoretical model calculations, some of which have been presented in the previous chapter. Recently also computer simulations have contributed to the field, representing a third way of approach to scientific investigation. In this chapter the simulation method used in the thesis is reviewed.

4.1 Overview of modelling at different length-scales

The description of materials greatly depends on the relevant length-scales. The behaviour of a cluster of atoms can be fundamentally different from that of a macroscopic piece of material. Different natural length-scales can be defined by studying particular aspects of the material in question. With increasing length-scale, the modelling involves coarse-graining, in which properly chosen degrees of freedoms are effectively integrated out, while keeping some of the essential, relevant properties. Recently the ambitious project of multi-scale modelling attempts to unify different levels of modelling [56].

At the microscopic length-scale – at atomistic level – the material is governed by the laws of quantum mechanics. Whether one uses the Schrödinger equation or the relativistic Dirac equation, the full quantum mechanical solution, even for a small number of particles, is practically unreachable. The Born-Oppenheimer approximation, based on the decoupling of the wave-function for the nucleus and electrons, represents a significant reduction of the general problem, to the subproblem of the nuclei, the electronic degrees of freedom being solved for fixed nuclei. The introduction of density-functional theory (DFT) has represented a break-

through in calculation of electronic structure of materials. In the density functional theory the quantum mechanical problem is concentrated on the determination of a single electronic density function $\rho(r)$ rather than the atomic wave-functions. Once the electronic density function is known the properties of the system are uniquely defined. Density functional methods are directly capable of high precision *ab initio* calculation of certain ground state properties, lattice parameter, cohesive, surface, stacking-fault energies. In its current state DFT can describe for example dislocation cores in silicon with high accuracy.

The next step in coarse-graining is the atomic-scale simulation by using the Molecular Dynamics (MD) method with a number of atoms ranging from several thousands to millions. In the MD method the electronic degrees of freedom are eliminated, which leads to a reduced problem of the classical equations of the motion for the atoms, namely for the nuclei. The quantum mechanical nature is represented by the interatomic potential. Typical length scales of the MD method are of the order of $10^{-7} - 10^{-9}$m and it operates in the pico-second timescale. The MD method is ideal for investigating the atomistic aspects of dislocations, such as core structure, extended dislocations and individual defect-dislocation interaction. The applicability of MD to study large systems is demonstrated for instance in the study of the interaction and dislocation reactions of two dissociated dislocations [57] and dislocation processes in a nanocrystalline materials [58], where the MD method was used with parallel computation for simulating a system consisting of several million particles. MD methods can give insight into short-ranged atomistic processes but when increasing length-scales they are ultimately limited due to computational requirements.

In the next level of coarse-graining i.e. in the mesoscopic range of description, from μm to 100μm, several methods have been developed for micro-structure and dislocation modelling. One of them is the Kinetic Monte-Carlo [59] method, which utilizes parameters obtained from atomistic calculations such as energy barriers for dislocation motion and kink-pair formation energy, is capable of modelling the 10^{-6}m length-scale and second time-scale. At this mesoscopic level of coarse graining one also considers Dislocation Dynamics (DD) which is a general term for modelling large-scale evolution of dislocation structure and in which dislocation segments are interacting with long-range elastic fields and forces are calculated from the Peach-Koehler formula, [60, 61]. The challenges for this method is the representation of short-ranged interactions. Furthermore, there are phase-field models for the collective motion of dislocations [62, 63], which have recently been gaining popularity.

Finally the macroscopic description of deformation of material relies on continuum elastic medium description, the most common numerical method being the Finite Element Method [64] for the description of elastic medium. Plastic prop-

erties are incorporated by constitutive equations that phenomenologically connect the relation between stress and strain of the systems under deformation.

4.2 Many-body potentials in the MD method

The Molecular Dynamics method studies a model system by solving numerically its equations of motion. Therefore the interatomic potential describing the material in question is crucial. The earliest interatomic potentials studied have been the Morse and Lennard-Jones pair-potentials, the latter originally developed for noble gases [65]. Later on, other potentials based on sophisticated calculations, such as the Dagens potential [66] derived from pseudo-potential theory have been developed. Still, pair-potentials have serious drawbacks, even at a practical level, which question their usefulness. A first problem concerns the elastic constants: by using pair-potentials the "Cauchy-relation" between the C_{12} and C_{44} elastic constants, $C_{12} = C_{44}$, is forced, which often contradicts experimental facts. The other and even more significant disadvantage of pair-potentials is that they are not capable of reproducing the basic properties of metallic bonding. In pair-potentials the bonding between two atoms does not depend on the environment whereas in reality bonding does depend on the position and number of neighbouring atoms. This problem of metallic cohesion manifests itself for example in the incorrect description of the surface energy, as pair-potentials would wrongly predict an outward relaxation and furthermore fail to account for the correct vacancy formation energy.

Since the 80's, a number of many-body potentials have appeared and replaced conventional pair-potentials in computational materials research when using MD simulations. Even though different many-body potentials have been developed from different physical approaches, the general expression for the cohesive energy of a mono-atomic material takes the following form,

$$E_{coh} = \frac{1}{2} \sum_{i \neq j} U(r_{ij}) + \sum_i F(\rho_i) \,, \qquad \rho_i = \sum_j f(r_{ij}) \,. \tag{4.1}$$

The cohesion energy of the crystal consists of two terms, the first one is the usual central-force pair-potential term and the second one is dependent on the particular local environment of the atoms. Both the pair-potential function $U(r_{ij})$ and the density function $f(r_{ij})$ depend solely on the magnitude of the distance of atoms i and j and not the orientation.

From different physical pictures different types of many-body functions have been developed which nevertheless have the same energy form. Among the various potentials, we mention the Effective Medium Theory (EMT) potential [67], the glue potential [68], and furthermore the Finnis-Sinclair (FS) and Embedded Atom

Method (EAM) potentials, which are used and dealt with in more detail in Publications II-VI. Generally most of these many-body potentials, with the exception of EMT in which theoretically all parameters can be obtained from ab initio calculations, are semi-empirical in nature. This means that although the general derivation is based on DFT, the actual parameters are determined by fitting to experimental data.

The idea behind the Finnis-Sinclair potential [69] is based on the second-moment approximation in the tight-binding potential scheme [70]. From the second-moment approximation it follows that the functional form of the many-body term in the total energy expression, Eq. (4.1), is explicitly a square-root function,

$$F(\rho_i) = a\sqrt{\rho_i} \,. \tag{4.2}$$

This means that the embedding function scales with the coordination number as $F \sim \sqrt{N}$, whereas for the pair-potentials $F \sim N$, so that the strength of the bonding scales with the coordination number as $1/\sqrt{N}$. Originally this potential was developed for bcc transition metals: one of the particular parametrization of the Finnis-Sinclair potential has been developed by Sutton and Chen [71] (SC-potential) for studying metallic clusters of both fcc and bcc materials and alloys [72]. It has been used to study dislocations in Publication VI.

The EAM potential was developed by Baskes, Daw and Foiles [73, 74, 75]. The physical principles behind the EAM model rely on the concept of jellium, a continuous electron density with a uniform neutralizing background charge. In the EAM it is assumed that the total cohesive energy is expressed in terms of embedding energy, that is the energy of an atom placed in the jellium created by neighbouring atoms. In this context the density in Eq. (4.1) can be interpreted as the electronic charge density, and the pair-potential as a Coulomb interaction term. Mathematically and conceptually the EAM formalism can be derived from density functional theory [76]. One of the reasons behind the success and popularity of the EAM potentials is their flexibility. Being semi-empirical in nature, the form of the cohesion energy is based on physical principles but the parametrization of the functions are determined by fitting to experimental material parameters or parameters determined from *ab initio* calculations. The embedding function $F(\rho)$ is usually determined indirectly, typically from the equation of state, that is the pressure-volume relation of the metal. EAM potentials are most suitable for close-packed materials with s p bonding and almost filled or empty d bands. There has been some attempt to extend EAM to covalent bonding materials [77]. For a review of EAM potentials and their applications see the review of Ref. [78]

There are a wealth of realizations of potential forms depending on which phenomenon is modeled. Usually there are some basic properties, such as the binding

energy, lattice and elastic constants and equation of state which are fitted. Parameters not used in the fitting are determined from the potential and compared to experimental data to validate the correctness of the potential. These might include surface properties, vacancy and interstitial formation energy, phonon spectra, crystal phase stability diagrams, stacking-fault energies, etc. It is also possible to use not an exact but rather a weighted, optimized fitting for wide range of parameters depending on their importance [79].

The EAM potential developed by Chantasiriwan and Miltsten incorporates elastic moduli up to the third order [80, 81]. Higher order elastic moduli can be important in case of large distortion of the crystal, present for example in dislocation cores. However, the original form of these potentials is not suitable for dislocation studies and needs to be corrected because of the negative stacking-fault energy predicted. This problem is addressed and studied in Publication II.

4.3 MD simulation techniques

4.3.1 Equations of motion

The classical Molecular Dynamics method is one of the earliest and still commonly used methods of atomistic simulations. The set of equations of motion for a classical mechanical systems of N interacting particles reads as follows,

$$\frac{d^2}{dt^2}[m\mathbf{r}_i] = -\nabla_{\mathbf{r}_i} E_{\mathrm{tot}} = \mathbf{F}_i \qquad \text{with} \qquad i = 1, \ldots, N \, , \qquad (4.3)$$

where E_{tot} is the total cohesive energy. The interatomic potential is determined from physical principles and by using the many body force-field of Eq. (4.1), the force $\mathbf{F}_i$ on atom i is explicitly

$$\mathbf{F}_i = - \sum_{j=1 \, (j \neq i)}^{N} \left\{ [F'(\rho_i) + F'(\rho_j)]f'(r_{ij}) + V'(r_{ij}) \right\} \frac{\mathbf{r}_{ij}}{r_{ij}} \, . \qquad (4.4)$$

From the computational point of view many-body potentials do not represent a significant increase in computational time compared to pair-potentials, since the total energy and forces are calculated using two cycles instead of one. In order to reduce the computational time, especially in the case of complicated functional forms of the energy expression, efficient table look-up methods are used [85]. Most of the basic techniques are now standard text-book methods and details can be found for example in Refs. [65, 86].

The integration of the equations of motion are carried out using a stable integration scheme that is often the velocity-Verlet algorithm,

$$
\begin{aligned}
\mathbf{r}(t + \Delta t) &= \mathbf{r}(t) + \mathbf{v}(t)\Delta t + \frac{1}{2}\mathbf{a}(t) \cdot (\Delta t)^2 \,, \\
\mathbf{v}(t + \Delta t) &= \mathbf{v}(t) + \frac{1}{2}\Big[\mathbf{a}(t) + \mathbf{a}(t + \Delta t)\Big] \cdot \Delta t \,.
\end{aligned}
\tag{4.5}
$$

The atomic positions, at time-step $t + \Delta t$ are calculated starting from the positions, velocities and forces (accelerations) at time t. Then the forces are calculated from Eq. (4.4) at time $t + \Delta t$. Finally the velocities at $t + \Delta t$ are calculated using both the forces (accelerations) at time t and $t + \Delta t$.

For constant temperature simulations a Nosé-Hoover thermostat has been used in the present work coupled with the Verlet integration algorithm. The relaxation of the system is carried out by including a simple damping method, i.e. one sets $\mathbf{v} = 0$, when $\mathbf{f} \cdot \mathbf{v} < 0$, meaning that the force acting on the particle is opposite to its velocity. In order to obtain accurate relaxed configuration an annealing method is used with alternating constant temperature and damping regimes.

4.3.2   Simulation set-up and boundary conditions

The orientation of the simulation cell we have used for studying dislocations in fcc metals corresponds to the natural geometry of the dislocation and its glide plane, i.e. we have chosen $\langle 110 \rangle$, $\langle 112 \rangle$, $\langle 111 \rangle$ as principal axes. In this way the dislocation line, and the glide direction is along the axis $\langle 110 \rangle$ and $\langle 112 \rangle$ depending on the type of dislocation.

Boundary conditions play a key role in simulations of dislocations. A traditional way to approach the problem is to use fixed boundary conditions. Namely, while periodic boundary conditions are applied along the dislocation line, atoms in some planes or shells at or near the boundaries are kept fixed. The presence of fixed atoms represents the bulk crystal. This type of boundary condition has the effect that the wall of fixed atoms exerts an image force on dislocations, analogously to classical electrodynamics. From text-book calculations the image force per unit length is long-ranged as it depends inversely on the distance, $F/L \sim 1/r$, and for a fixed boundary it is repulsive. In case of a free surface a similar attractive force appears. In order to minimize the effect described above flexible boundaries conditions [87] have been developed which can correct the effect of fixed boundaries on the dislocation properties and make it possible to carry out simulations with smaller system sizes.

Periodic boundary conditions are widely used in all areas of computer simulations to model an infinite sized material. Full periodic boundary conditions for a
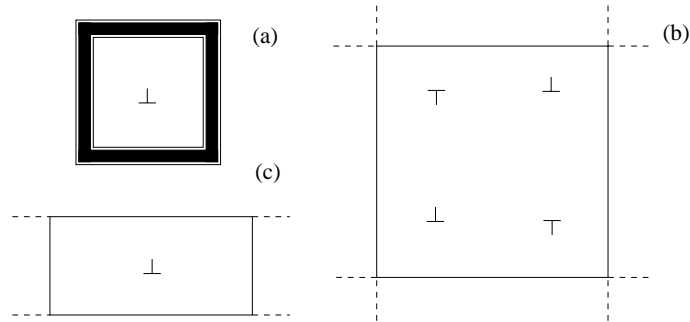
Figure 4.1: Schematic representation of different types of boundary conditions: (a) Fixed boundary conditions, (b) full periodic boundary conditions with quadrupole dislocation arrangement, (c) dislocation array type of boundary conditions.

dislocation represent a special problem as it is required that the net Burgers vector of the simulation cell should be zero, because it would correspond to an infinite energy of the system. The actual realization of the model system is either a dipole or quadrupole.

The third type of boundary condition uses a single dislocation and periodic boundary conditions both along the dislocation line and the glide direction whereas in the third direction the boundary is semi-free, that is atoms can freely move in the surface plane, but are fixed in the third direction. This is the so-called periodic array of dislocation boundary condition, because the model system corresponds to an infinite array of dislocations. This type of boundary condition has been used by Baskes and Daw [78] and has recently become popular in simulations for dislocation-obstacle interaction. Several properties of this type of boundary condition, static and dynamical ones, have been recently reviewed by Osetsky and Bacon [88].

4.3.3 Visualization and defect identification

There are several methods for identification and visualization of dislocations and other lattice defects. One of the most conventional methods of visualization is based on the potential energy. Since in the dislocation core the lattice structure is highly distorted, atoms in that region have a significantly higher potential energy than in the undisturbed perfect crystal. Then by setting an energy barrier one can separate the dislocation core from other parts of the crystal. An alternative method is based on the geometry of the local atomic configuration, i.e. on how many atoms

are placed inside the first neighbour shell. Using the central symmetry parameter it is possible to identify both dislocations and stacking-faults which have low energy [89].

When the glide plane and the dislocation orientation is known, the measurement from the strain field can lead to an accurate determination of the dislocation position. The disregistry function is measured from atomistic calculations as the difference between atomic displacement above and below the plane that contains the dislocation, $\mathbf{f}(x) = \mathbf{u}^+(x) - \mathbf{u}^-(x)$, measured perpendicularly to the dislocation line. From the measured disregistry function, using fitting to a simple analytical form such as for example Eq. (3.9), the position of the dislocation can be determined.

4.4 Previous MD studies of dislocation properties

Computer simulations have long been used for studying the structure of dislocations. Several studies concentrated on the perfect dislocation splitting into Shockley partials [90, 91, 92, 93, 94, 95]. These studies include the determination of internal structure of the dissociated dislocation through the disregistry function, the separation distance and core width and its comparison with the theoretical estimates based on elasticity theory and the Peierls-Nabarro model. As related phenomena the role of dislocations in diffusion [90, 91, 95] and cross-slip processes [92, 93] have also been investigated.

Additionally, MD simulations have been used to compute the mobility of dislocations in different materials and several methods for determining the Peierls stress have been employed. The simplest method is to move the dislocation by applying either shear strain or shear stress resolved on the glide plane. The point at which the dislocation starts to move gives the value of the critical resolved shear stress (CRSS) which is the minimum stress to move a dislocation over a lattice constant. At zero temperature case this is identified with the Peierls stress [93, 94]. In a simulation set-up with fixed boundary conditions the dislocation can be moved by shear strain, but in contrast to the previous case, the dislocation will move to a new equilibrium position rather than keep its motion, because of the presence of image forces due to the fixed boundaries. From the assumption that the image force is linear, the Peierls stress can be determined, see e.g. Ref. [95]. This method has been used in Publications IV and V. It is also possible to estimate σ_{PN} in an approximative way, by a static method similar to the Peierls-Nabarro model. An atomic configuration is generated corresponding to the dislocation disregistry profile translated along the glide direction and the energy of the configuration, $W(x)$ is measured. From the variation of the energy the maximum stress, using Eq. (3.10)

is determined, see Ref. [96].

Recently, the interaction process of a moving dislocation with defect clusters studied by MD simulations has attracted much interest. The main advantage of numerical simulations, compared to analytical calculations, is the ability to treat core-core interactions realistically. Studies of this kind concern defects formed both by interstitials [97] and vacancies, for which an important example is the interaction of a vacancy type SFT with glissile dislocations in fcc crystals. While previous works concentrated on the processes of SFT and edge dislocation intersection [98, 99], in Publication VI the properties of the interaction with a dissociated screw dislocation are studied.

Chapter 5

Summary of results

This chapter contains an overview of the main results of this thesis both concerning the instability in brittle fracture and those concerning the dissociated dislocations in fcc structure, together with a description of their static or dynamics properties.

5.1 Crack branching instability

Publication I deals with the study of anisotropy in the Born-Maxwell fracture model illustrated in Chapter. 2. The anisotropy was introduced in the model by modifying the elastic parameters α and β either in a symmetric or along a diagonal direction with respect to the main crack line and it is characterized by a single parameter k. The effect of anisotropy was studied in two respects, the fracture pattern formation and the power spectra of the crack tip velocity. In the symmetrical anisotropy case the branching shows a dependence on the anisotropy parameter, such that increasing k leads to an increase in the spatial period of daughter cracks. Near the isotropic case, when $k \approx 1$, the branching phenomenon can be understood through scaling concepts. As the velocity of the crack increases, due to its dependence on k, the spatial period of daughter cracks increases but the frequency of oscillations remains the same. In case of stronger anisotropy the branching shows a more complex behaviour. In the diagonal case the reflection symmetry is broken and there are two different side-branch structures on the two sides of the main crack. The changes in the fracture pattern is show in Fig. 5.1. Concerning the power spectrum of the crack tip velocity, in the symmetrical anisotropy case the frequency depends monotonically but not trivially on k. In the diagonal case the main frequency is dictated by the side, which has a longer period, whereas the other side only gives rise to minor effect.

Despite the limits of the present mesoscale model, the main features of crack
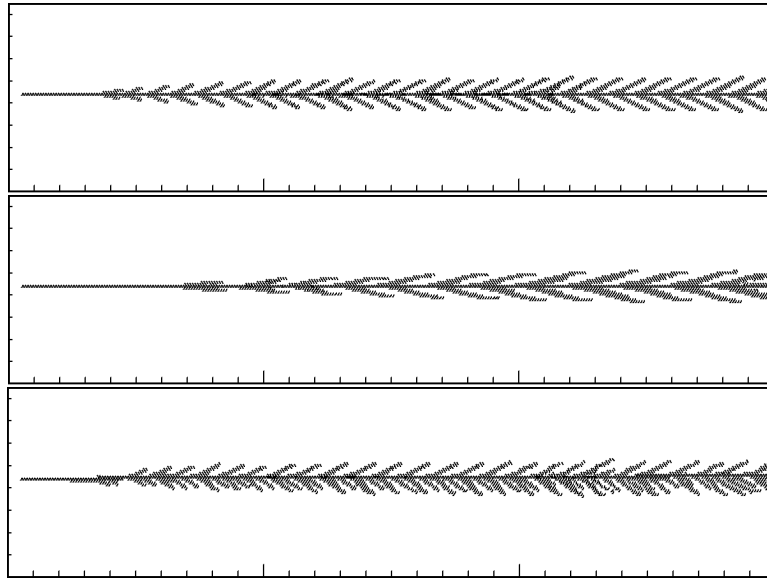
Figure 5.1: From top to bottom: fracture patterns in a isotropic system, in a system with symmetrical isotropy, and with diagonal isotropy (from Publication I).

branching phenomenon is modeled reasonably well. In fact, while the general structure of the model is motivated by experimental facts, the model itself does not correspond to any particular material.

5.2 Interatomic potential

When looking for a reliable interatomic potential, the detailed features of the material under investigation have to be taken into account, since they have a relevant role. In Publication II by using the atomistic Molecular Dynamics method the dissociation process of an edge dislocation splitting into two partials is investigated. It was found that the boundary conditions may sensitively affect the dislocation structure. The main observation was, however, that the inter-atomic potential developed by Chantasiriwan and Milstein [81] provides a negative intrinsic stacking-fault energy and incorrectly favors the hcp over the fcc structure. This means that dissociated dislocations would be unstable and no equilibrium separation would be achieved. Thus the potential in its original form is not suitable for dissociated dislocation studies. The potential has otherwise excellent elastic properties, as it incorporates elastic moduli up to third order, and predicts correctly the bcc-fcc

phase stability. In order to resolve the problem of the negative stacking-fault, in Publication II a correction to the potential was suggested based on changing the cut-off range, and reiterating the fitting of parameters until a positive stacking-fault energy is obtained.

The systematic development of a corrected potential is carried out in Publication III for four fcc metals: Al, Au, Ni and Cu. The main emphasis is on the potentials being able to reproduce reasonable stacking-fault energies so that they can be used in simulations of extended dislocations. To this aim the cut-off of the interatomic potential was varied. This cut-off changing method was aimed at getting reasonable stacking-fault energies. It should be noted that a long-ranged potential is necessary in the EAM scheme to obtain stacking-fault energies as a short-ranged potential would lead to no difference between the hcp and fcc phases. For different type potentials more systematic types of fitting are available, such as that based on the tight-binding model where higher-order terms can be related to the stacking-fault energy. By repeating the fitting procedure new sets of parameters were obtained and additionally for two materials the functional form of the pair potential was modified. Several properties of the corrected potential were calculated to validate the result including the stacking-fault, point-defect and surface energies as well as phonon spectra. The quality of the above mentioned scheme varies depending on the specific potential but the general result is good and comparable to those using similar EAM potentials, despite some trade-offs in cut-off distance tuning made to obtain the best fit for experimental phonon data. For two materials the phonon spectra is slightly modified at the boundary of the Wigner-Seitz cell. The corrected potential for the case of Ni, developed in Publication III, has been used as the basis for all the subsequent MD simulations in Publication IV, V and VI.

5.3   Dislocation core structure and Peierls stress

Let us now consider both the static and dynamical properties of dissociated dislocations. The detailed analysis of the static structure of a dissociated $\frac{1}{2}\langle 110 \rangle$ type dislocation for both edge and screw orientation was presented in Publication IV. There we chose Ni as the material of interest because it has a relatively small separation distance between partials and possibly overlapping core-structure that could show interesting results. The edge and screw dislocations are qualitatively different: in the case of the dissociated edge dislocation the separation distance is large and the partials can be represented as individual dislocations and a Volterra type description is appropriate. The dissociated screw dislocation represents an intermediate case where the two partials are still identifiable as individual peaks in the
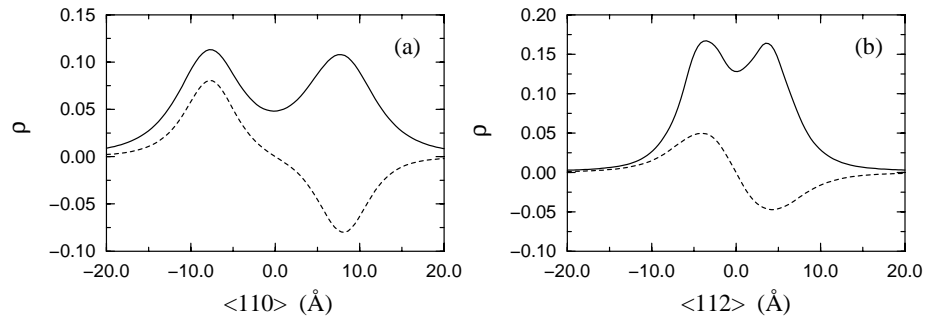
Figure 5.2: The misfit function describing the local density of Burgers vector for (a) dissociated edge and (b) dissociated screw dislocation. Solid lines denote the edge component of the edge and the screw component of the screw dislocation. Dashed lines denote the screw component of the edge and the edge component of the screw dislocation. (Publication IV)

misfit function, but their cores are strongly overlapping. This overlap is manifested for example in the dissociation path, as a reduction of the maximum edge component of the Burgers vector, which was observed in several simulation works. A general observation is that the comparison of the simulation results with those of model calculations, both for the separation distance given by the elasticity theory and the core width given by the Peierls model, is fairly adequate. This probably happens because the partial dislocations have typically a wide dislocation core. The analytic functional form of the misfit function shows an even better agreement with numerical results if the non-zero distance from the glide-plane is taken into account for both the screw and edge dislocation orientation.

A simple estimate of the Peierls stress was provided by applying a strain increment on the dislocation, in a quasi-static way similarly to Ref. [95]. One qualitative result is that the edge dislocation has a significantly higher mobility than the screw one. We also found that the relation between the equilibrium separation distance and the period of the Peierls potential a' may lead to interesting effects. In the edge case the partials were found to move in-phase with respect to the underlying crystal structure felt by the dislocation, as $d \approx 12a'$. On the other hand in the case of screw dislocation they move in opposite phase, d being a half-integer multiple of a'. This leads to some fluctuations in the separation distance and a decrease in the effective Peierls stress. The fact that the screw dislocation has a separation distance about a half-integer multiple of the Peierls potential d is possibly particular for the applied potential but this supports the hypothesis that the ratio of separa-

tion distance and the period of the Peierls potential d/a' bears significance for the structure of the dislocation.

Motivated by the findings of Publication IV, we were inspired to study a generalized case of dissociated screw dislocation moving in the Peierls potential by using extensive and systematic computer simulations which are presented in Publication V. The basic idea was to investigate a dislocation with varying separation distance, i.e. where the ratio d/a' can change. Technically, in the simulations this variation of the separation distance was achieved by changing the external stress, whereas in reality it is realized by point defects or other impurities modifying the stacking-fault energy. Here we made a more careful analysis than in Publication IV by distinguishing between the edge and screw components of the partials in the dissociated dislocation, which turned out to behave slightly differently concerning already the equilibrium separation distance. When the dislocation moves the change in internal structure can be characterized by the separation distance and the core width. The fluctuation of the separation distance is sensitive to the d/a' ratio, the largest fluctuation being observed in the half-integer case. As for the core width the fluctuations arise as a result of both the underlying periodic potential and the internal fluctuation. The effects obtained are similar to analytic model calculations. The fluctuations in the separation distance are qualitatively similar to those observed in the model of coupled mass points moving in a periodic potential and the Volterra model of the dissociated dislocation studied by Schoeck and Püschl [55]. The fluctuations in the core width was studied in the variational Peierls-Nabarro model [43]. While the changes in the internal structure of the dislocation represents a rather theoretically oriented question the effective Peierls-stress bears practical significance related to the dislocation mobility, as explained in the previous chapters.

The main result of Publication V is about the measurement of the dependence of the effective Peierls stress on the separation distance. The overall result is that dislocations with significant core overlap, but with still identifiably partials, show a measurable variation in the effective Peierls stress. Although the fluctuation of the effective Peierls stress can be a large factor it is possibly too small to explain the two orders of magnitude discrepancy in the two estimates of the Peierls stress alone.

5.4 Dislocation-defect interaction

Following the studies of the properties of dissociated dislocations, in Publication VI the interaction of a moving dissociated dislocation with a stacking-fault tetrahedron, one of the most common defects in irradiated materials, is investigated. Cur-
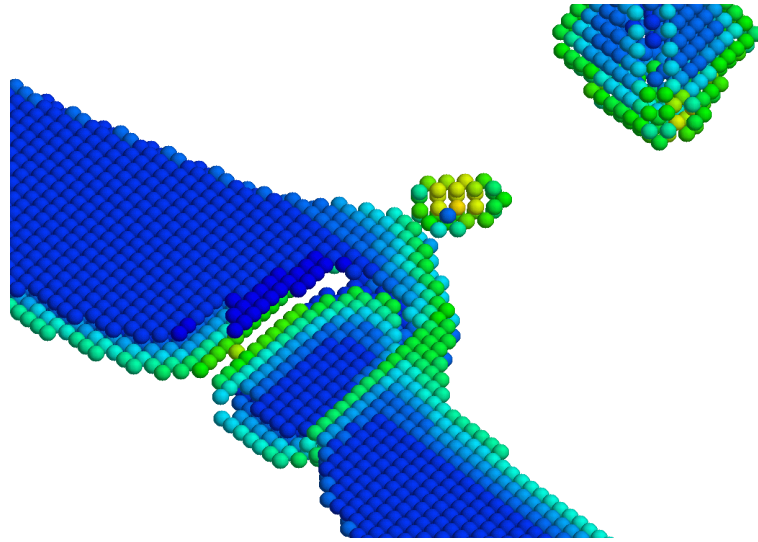
Figure 5.3: A dissociated screw dislocation containing jog line after the interaction with SFT. The central symmetry parameter is used. Atoms in dislocation core are denoted with green and in stacking-fault region with blue color.

rently there are only examples of simulation studies concerning the intersection of an edge dislocation and a SFT [98, 99]. Here the interaction of a dissociated screw dislocation with a perfect SFT is studied and several aspects of the process are analyzed. These factors include the orientation of the defect, the relative position of the defect and dissociated screw dislocation and the stacking-fault energy. When the dislocation intersects the SFT in the middle several times, it can separate the defect into two parts. On the other hand, when the glide plane coincides with the base of the SFT, the intersection process shows a variety of dislocation interactions, jog line formation and bending. These are particularly well observable in the case of the model system with the low stacking-fault energy. For a SFT with a smaller size, the critical resolved shear stress for the dissociated dislocation to pass through the defect is determined and it was observed that this quantity is rather independent of both the interatomic potential and the defect orientation. It is shown that in special cases the screw dislocation can absorb vacancies by jog formation, in contrast to the previous study [98] where the jog formation was observed only for truncated SFTs, and possibly destroy the SFT by multiple intersection, similarly to the findings of experimental studies [100].

Bibliography

[1] W. D. Callister. *Materials Science and Engineering: An Introduction*. Wiley and Sons, fifth edition, 2000.

[2] L. B. Freund. *Dynamic Fracture Mechanics*. Cambridge University Press, first edition, 1998.

[3] R. W. Hertzberg. *Deformation and Fracture Mechanics of Engineering Materials*. Wiley, fourth edition, 1995.

[4] J. Fineberg, S. P. Gross, M. Marder, and H. Swinney. Instability in dynamic fracture. *Phys. Rev. Lett*, 67:457, 1991.

[5] J. Fineberg, S. P. Gross, M. Marder, and H. Swinney. Instability in the propagation of fast cracks. *Phys. Rev. B*, 45:5146, 1992.

[6] E. Sharon, S. P. Gross, and J. Fineberg. Local crack branching as a mechanism for instability in dynamic fracture. *Phys. Rev. Lett.*, 74:5096, 1995.

[7] E. Sharon and J. Fineberg. Microbranching instability and the dynamic fracture of brittle materials. *Phys. Rev. B*, 54:7128, 1996.

[8] J. Fineberg and M. Marder. Instability in dynamic fracture. *Physics Reports*, 313:1, 1999.

[9] F. F. Abraham, D. Brodbeck, R. A. Rafey, and W. E. Rudge. Instability dynamics of fracture: A computer simulation investigation. *Phys. Rev. Lett.*, 73:272, 1994.

[10] P. Gumbsch, , S. J. Zhou, and B. L. Holian. Molecular dynamics investigation of dynamic crack stability. *Phys. Rev. B*, 55:3445, 1997.

[11] B. L. Holian and R. Ravelo. Fracture simulations using large-scale molecular dynamics. *Phys. Rev. B*, 51:11275, 1995.

[12] J. Åström and J. Timonen M. J. Alava. Crack dynamics and crack surfaces in elastic beam lattices. *Phys. Rev. E*, 57:R1259, 1998.

[13] P. Heino and K. Kaski. Mesoscopic model of crack branching. *Phys. Rev. B*, 54:6150, 1999.

[14] M. Born and K. Huang. *Dynamical Theory of Crystal Lattices*. Oxford University Press, first edition, 1968.

[15] H. J. Hermann and S. Roux eds. *Statistical Models for the Fracture of Disordered Media*. Elsevier North Holland, first edition, 1990.

[16] T. T. Rautiainene and K. Kaski M. J. Alava. Dissipative dynamic fracture of disordered systems. *Phys. Rev. E*, 51:R2727, 1995.

[17] J. P. Hirth and J. Lothe. *Theory of dislocations*. Wiley, second edition, 1982.

[18] M. Polanyi. *Z. Physik*, 89:660, 1934, E. Orowan *Z. Physik*, 89:634, 1934, G.I. Taylor *Proc. Roy. Soc.*, A145:362, 1934.

[19] F. R. Nabarro. *Theory of crystal dislocation*. Oxford University Press, first edition, 1982.

[20] U. F.Kocks and H. Mecking. Physics and phenomenology of strain hardening: the fcc case. *Progress in Materials Science*, 48:171, 2003.

[21] D. Kuhlmann-Wilsdorf. The theory of dislocation-based crystal plasticity. *Phil. Mag. A*, 79:955, 1999.

[22] H. Kleinert. *Gauge fields in condensed matter*. World Scientific: Singapore, first edition, 1989.

[23] E. A. Fitzgerald. Dislocations in strained-layer epitaxy: theory, experiment and application. *Mat. Sci. Rep.*, 7:87, 1991.

[24] F. Cleri, D. Wolf, S. Yip, and S. R. Phillpot. Atomistic simulation of dislocation nucleation and motion from a crack tip. *Acta Mater.*, 45:4993, 1997.

[25] D. Hull and D. J. Bacon. *Introduction to dislocations*. Pergamon Press Ltd, third edition, 1984.

[26] L. J. Teutonico. The dissociation of dislocations in the face-centered cubic structure. *Acta Metallurica*, 11:1283, 1963.

[27] L. J. Teutonico. Dislocations in the primary slip system of face-centered cubic crystals. *Acta Metallurgica*, 11:391, 1963.

[28] N. L. Peterson. Self-diffusion in pure metals. *Journal of Nuclear Materials*, 69-70:3, 1978.

[29] J. P. Hirth. Some current topics in dislocation theory. *Acta. Mater.*, 48:93, 2000.

[30] M. Kiritani. Similarity and difference between fcc, bcc and hcp metals from the view point of point defect cluster formation. *Journal of Nuclear Materials*, 276:41, 2000.

[31] Y. Dai and M. Victoria. Defect structures in deformed f.c.c. metals. *Acta Mater.*, 45:3495, 1997.

[32] M. Victoria, N. Baluc, C. Bailat, Y. Da, M. I. Luppo, Schäublin, and B. N. Singh. The microstructure and associated tensile properties of irradiated fcc and bcc metals. *Journal of Nuclear Materials*, 276:114, 2000.

[33] J. S. Robach, I. M. Robertson, B. D. Wirth, and A. Arselis. In-situ transmission electron microscopy observations and molecular dynamics simulations of dislocation-defect interactions in ion-irradiated copper. *Phil. Mag.*, 83:955, 2003.

[34] L. Z. Sun, N. M. Ghoniem, and Z. Q. Wang. Analytical and numerical determination of the elastic interaction energy between glissile dislocations and stacking-fault tetrahedra in fcc metals. *Mat. Sci. Eng. A*, 309-310:178, 2001.

[35] M. Hiratani, H. M. Zbib, and B. D. Wirth. Interaction of glissile dislocatoins with perfect and trunctated stacking-fault tetrahedra in irradiated materials. *Phil. Mag A*, 82:2709, 2002.

[36] J. Frenkel and T. Kontorova. *Phys. Z. Sowjetunion*, 13:1, 1938.

[37] K. Ohsawa, H. Koizumi, H. O. K. Kirchner, and T. Suzuki. The critical stress in a discrete Peierls-Nabarro model. *Phil. Mag A*, 69:171, 1994.

[38] H. B. Huntington. Modification of the Peierls-Nabarro model for edge dislocation core. *Proc. Phys. Soc. B*, 68:1043, 1955.

[39] F. R. N. Nabarro. Theoretical and experimental estimates of the Peierls stress. *Phil. Mag. A.*, 75:703, 1997.

[40] B. Joós and M. S. Duesbery. The Peierls stress of dislocations: An analytic formula. *Phys. Rev. Lett.*, 78:266, 1997.

[41] G. Schoeck. The Peierls dislocation: line energy, line tension, dissociation and deviation. *Acta Mater.*, 35:2597, 1997.

[42] G. Schoeck. The dissociation energy of extended dislocations in fcc lattices. *Phil. Mag. A*, 79:1207, 1999.

[43] G. Schoeck. The Peierls energy revisited. *Phil. Mag. A*, 79:2629, 1999.

[44] G. Schoeck. The core structure, recombination energy and Peierls energy for dislocatins in Al. *Phil. Mag. A*, 81:1161, 2001.

[45] G. Schoeck. Normal and fractional kink pais in dissociated dislocations. *Phil. Mag. A*, 82:1033, 2002.

[46] O. N. Mryasov, Yu. N. Gornostyrev, and A. J. Freeman. Generalized stacking-fault energetics and dislocation properties: Compact versus spread unit-dislocation structures in TiAl and CuAu. *Phys. Rev. B.*, 58:11927, 1998.

[47] O. N. Mryasov, Yu. N. Gornostyrev, M. van Schilfgaarde, and A. J. Freeman. Complex evoolution of dislocation core structure in a process of motion model anaylsis with ab-initio parameterization. *Mat. Sci. Eng. A*, 309-310:138, 2001.

[48] V. V. Bulatov and E. Kaxiras. Semidiscrete variational Peierls framework for dislocation core properties. *Phys. Rev. Lett.*, 78:4221, 1997.

[49] N. Kioussis G. Lu, V. V. Bulatov, and E. Kaxiras. Generalized-stacking-fault energy surface and dislocation properties of aluminum. *Phys. Rev. B*, 62:3099, 2000.

[50] G. Lu and E. Kaxiras. Can vacancies lubricate dislocation motion in aluminum ? *Phys. Rev. Lett.*, 89:105501, 2002.

[51] A. H. W. Ngan. A new model for dislocation kink-pair activation at low temperatures based on the Peierls-Nabarro concept. *Phil. Mag A*, 79:1697, 1999.

[52] G. Fantozzi, C. Esnouf, W. Benoit, and I. G. Ritchie. Internal friction and microdeformation due to the intsinsic properties of dislocation: The Bordoni relaxation. *Progress in Materials Science*, 27:311, 1982.

[53] W. Benoit, M. Bujard, and G. Gremaud. Kink dynamics in f.c.c. metals. *Phys. Stat. Sol. A*, 104:427, 1998.

[54] G. Schoeck. The Peierls stress and the flow stress in fcc metals. *Scripta Merallurgica et Materiala*, 30:611, 1994.

[55] G. Schoeck and W. Puschl. Dissociated dislocations in the Peierls potential. *Mat. Sci.Eng. A*, 189:61, 1994.

[56] G. Lu and E. Kaxiras. Multiscale modelling of nanomechanics and micromechanics: an overview. *Phil. Mag.*, 83:3475, 2003.

[57] S. J. Zhou, D. L. Preston, P. S. Lomdahl, and D. M. Beazley. Large-scale molecular dynamics simulations of dislocation intersection in copper. *Science*, 279:1525, 1998.

[58] V. Yamakov, D. Wolf, S. R. Phillpot, and A. K. Mukherjee. Dislocation processes in the deformation of nanocrystalline aluminium by molecular-dyanmics simulation. *Nature Materials*, 1:45, 2002.

[59] W. Cai, V. V. Bulatov, S. Yip, and A. S. Argon. Kinetic Monte-Carlo modelling of dislocation motion in bcc metals. *Mat. Sci. Eng. A*, 309-310:270, 2001.

[60] V. V. Bulatov. Current developments and trends in dislocation dynamics. *Journal of Computer-Aided Materials Design*, 9:133, 2002.

[61] M. Verdier, M. Fivel, and I. Groma. Mesoscopic scale simulation of dislocation dynamics in fcc metals: Principles and applications. *Modelling Simul. Mater. Sci. Eng.*, 6:755, 1998.

[62] Y. U. Wang, Y. M. Jin, A. M. Cuiti no, and A. G. Khachaturyan. Nanoscale phase field microelasticity theory of dislocations: model and 3D simulations. *Acta Mater.*, 49:1847, 2001.

[63] D. Rodney, Y. Le Bouar, and A. Finel. Phase field methods and dislocations. *Acta Mater.*, 51:17, 2003.

[64] O. C. Zienkiewich and R. L. Taylor. *The Finite Element Method, Volume 1,2*. McGraw-Hill Book Company, fourth edition, 1994.

[65] M. P. Allen and D. J. Tildesley. *Computer Simulation of Liquid*. Oxford University Press, first edition, 1987.

[66] N. Q. Lam, L. Dagens, and N. V. Doan. Calculations of the properties of self-interstitials and vacancies in the face-centred cubic metals Cu, Ag and Au. *J. Phys. F*, 13:2503, 1983.

[67] K. W. Jacobsen, J. K. Norskov, and M. J. Puska. Interatomic interactions in the effective-medium theory. *Phys. Rev. B*, 35:7423, 1987.

[68] F. Ercolessi, E. Tosatti, and M. Parrinello. Au(100) surface reconstruction. *Phys. Rev. Lett.*, 57:719, 1986.

[69] M. W. Finnis and J. E. Sinclair. A simple empirical N-body potential for transition metals. *Phil. Mag. A*, 50:45, 1984.

[70] A. P. Sutton. *Electronic Strucuture of Materials*. Oxford University Press, first edition, 1994.

[71] A. P. Sutton and J. Chen. Long-range Finnis-Sinclair potentials. *Phil. Mag. Lett.*, 61:139, 1990.

[72] H. Rafii-Tabar and A. P. Sutton. Long-range Finnis-Sinclair potentials for f.c.c. metallic alloys. *Phil. Mag. Lett.*, 63:217, 1991.

[73] M. S. Daw and M. I. Baskes. Embedded-atom method: Derivation and application to impurities, surfaces, and other defects in metals. *Phys. Rev. B*, 29:6443, 1984.

[74] S. M. Foiles, M. I. Baskes, and M. S. Daw. Embedded-atom-method functions for the fcc metals Cu, Ag, Au, Ni, Pd, Pt, and their alloys. *Phys. Rev B*, 33:7983, 1986.

[75] M. S. Daw. Model of metallic cohesion: The embedded-atom method. *Phys. Rev. B*, 39:7441, 1989.

[76] M. Finnis. Interatomic forces in materials. *Progress in Materials Science*, 49:1, 2004.

[77] M. I. Baskes. Application of the embedded-atom method to covalent materials: A semiempirical potential for silicon. *Phys. Rev. Lett*, 59:2666, 1987.

[78] M. S. Daw, S. M. Foiles, and M. I. Baskes. The embedded-atom method: a review of theory and applications. *Materials Science Reports*, 9:251, 1993.

[79] Y. Mishin, D. Farkas, M. J. Mehl, and D. A. Papaconstantopoulos. Interatomic potentials for monoatomic metals from experimental data and ab initio calculations. *Phys. Rev. B.*, 59:3393, 1999.

[80] S. Chantasiriwan and F. Milstein. Higher-order elasticity of cubic metals in the embedded-atom method. *Phys. Rev. B*, 53:14080, 1996.

[81] S. Chantasiriwan and F. Milstein. Embedded-atom models of 12 cubic metals incorporating second- and third-order elastic-moduli data. *Phys. Rev. B*, 58:5996, 1998.

[82] F. Ducastelle and F. Cyrot-Lackman. Moments developments. ii. application to the crystalline structures and the stacking fault energies of transition metals. *J. Phys. Chem. Solids*, 32:285, 1971.

[83] V. Vitek. Intrinsic stacking-faults in body-centered cubic crystals. *Phil. Mag.*, 18:773, 1968.

[84] J. Hartford, B. von Sydow, G. Wahnström, and B. I. Lundqvist. Peierls barriers and stresses for edge dislocations in Pd and Al calculated from first principles. *Phys. Rev. B.*, 58:2487, 1998.

[85] D. Wolff and W. G. Rudd. Tabulated potentials in molecular dynamics simulations. *Comuter Physics Communications*, 120:20, 1999.

[86] D. Frenkel and B. Smit. *Understanding Molecular Simulation*. Academic Press, second edition, 2002.

[87] S. Rao, J. P. Simmons C. Hernandez, T. A. Parthasarathy, and C. Woodward. Green's function boundary conditions in two-dimensioinal and three-dimensional atomistic simulations of dislocations. *Phil. Mag.*, 77:231, 1998.

[88] Yu. N. Osetsky and D. J. Bacon. An atomic level model for studying the dynamics of edge dislocations in metals. *Modelling Simul. Mat. Sci. Eng.*, 11:427, 2003.

[89] C. L. Kelchner, S. J. Plimpton, and J. C. Hamilton. Dislocation nucleation and defect structure during surface indentation. *Phys. Rev. B*, 58:11085, 1998.

[90] J. Huang, M. Meyer, and V. Pontikis. Core structure of a dissociated easy-glide dislocation in copper investigated by molecular dynamics. *Phys. Rev. B*, 42:5495, 1990.

[91] J. von Boehm and R. M. Nieminen. Molecular-dynamics study of partial edge dislocations in copper and gold: Interactions, structures, and self-diffusion. *Phys. Rev. B.*, 53:8956, 1996.

[92] T. Rasmussen, K. W. Jacobsen, T. Leffers, and O. B. Pedersen. Simulations of the atomic structure, energetics, and cross slip of screw dislocations in copper. *Phys. Rev. B*, 56:2977, 1997.

[93] M. S. Duesbery. Dislocation motion, constriction and cross-slip in fcc metals. *Modelling Simul. Mater. Sci. Eng.*, page 35, 1998.

[94] B. von Sydow, J. Hartford, and G. Wahnström. Atomistic simulations and Peierls-Nabarro analysis of the Shockley partial dislocations in palladium. *Comp. Mat. Sci*, 15:367, 1999.

[95] Q. F. Fang and R. Wang. Atomistic simulation of the atomic structure and diffusion within the core region of an edge dislocation in aluminum. *Phys. Rev. B*, 62:9317, 2000.

[96] P. Gumbsch R. Schroll, V. Vitek. Core properties and motion of dislocations in NiAl. *Acta Mater.*, 46:903, 1998.

[97] D. Rodney. Molecular dynamics simulation of screw dislocation interacting with interstitial frank loops in a model fcc crystal. *Acta Mater.*, 52:607, 2004.

[98] T. Diaz de la Rubia B. D.Wirth, V. V. Bulaton. Dislocation-stacking fault tetrahedron interactions in Cu. *Journal of Engineering Materials and Technology*, 124:329, 2002.

[99] Yu. N. Osetsky, R. Stoller, and Y. Matsukava. Dislocation-stacking fault tetrahedron interaction: what can we learn from atomic-scale modelling. *Journal of Nuclear Materials*, 329-333:1228, 2004.

[100] Y. Matsukawa and S. J. Zinkle. Dynamic observation of the collapse process of a stacking-fault tetrahedron by moving dislocations. *Journal of Nuclear Materials*, 329-333:919, 2004.

Enclosed Publications